Time Correlated Gamma-ray Spectroscopy of the Shell Model Nucleus ^{213}Ra

Thomas Palazzo

A thesis submitted for the degree of
Bachelor of Science with Honours in Physics of
The Australian National University

October, 2015

Declaration

This thesis is an account of research undertaken between February 2015 and October 2015 at The Research School of Physics and Engineering, College of Physical and Mathematical Sciences, The Australian National University, Canberra, Australia.

Except where acknowledged, the material presented in this thesis is, to the best of my knowledge, original and has not been submitted in whole or part for a degree in any university.

Thomas Palazzo

October, 2015

Preface

This thesis reports on an honours project carried out in the Department of Nuclear Physics at the ANU utilising the 14UD particle Accelerator. The aim of the project was to populate high-spin states in the nucleus ^{213}Ra and use the CAESAR detector array to perform time correlated γ-ray spectroscopy to determine the nuclear level scheme. In addition to this, throughout the year I have actively contributed to the γ research group participating in the following experiments:

1. an investigation High-K isomers in ^{174}Re with international visitors
2. Dr. Tibor Kibedi's study of the following nuclei: ^{54}Fe, ^{140,142}Ce, ^{58,60,64}Ni and the observation of the Hoyle state in ^{12}C
3. Dr Sankha Hota's investigation of high spin states in ^{215}Ac
4. Matt Gerathy's experiment investigating ^{182}W
5. and, Aqeel Akber's fast timing measurements of short-lived isomers in ^{188}Pt using $LaBr_3$ detectors.

I also attended the international HIAS 2015 conference where I presented an abstract and poster summarising my results.

Except where stated the contents of this thesis are entirely my own work.

Acknowledgements

The past year has been an incredible time and I would like to thank Gregory Lane and Andrew Stuchbery for always answering my (constant) questions and allowing me to undertake my honours research in the Department of Nuclear physics at the ANU. I would like to also extend my gratitude to A. J. Mitchell, S. S. Hota and M. W. Reed for immediately assisting me throughout the year whenever I came to them for help.

To the Ph.ANUS2015 (Physics honours ANU students) cohort you guys were great! I will not forget the hour long lunch time discussions at Fellows after the arduous mornings of class *or* the continuous stream of snapchats and facebook messages to keep me distracted from my work throughout the day. On the subject of Fellows I would like to thank Ben, Rosie, Edyl and all the others for supplying me with food and caffeine (best and cheapest coffee on campus) throughout the day. Thank you for putting 20% cold water in my coffee and thank you for asking the chefs every day if there were any mushrooms (blegh!) in the food, sorry I was such a demanding customer.

To Frank, Ken, Camilla and Ellen and all my other friends, thank you for putting up with me in my (very occasionally) grumpy and exhausted state. Thank you for distracting me when I was bored and listening to my complaints when I was frustrated. Thank you for explaining to me of how to equip my scarf whenever I forgot. To Frank in particular, thank you for driving me home several times a week. At this stage i owe you about 47 cups of coffee.

It is perhaps unorthodox but I would also like to extend my thanks to Louis C.K., Dave Chappelle and many other comedians for all the nights where I gave up on productivity and decided I needed a good laugh instead. I would like to thank Jimi Hendrix, Pink Floyd, Eric Clapton (the list goes on) for providing me with music to make the days (and days and days and days) of looking at spectra slightly more enjoyable.

To my family, thank you for the free roof over my head, free food, free internet and occasional use of the (***my***) car. This thesis would not have been possible without your continuous support. I hope I have made you proud.

Abstract

This thesis reports the observation of high-spin states in ^{213}Ra made via the ^{204}Pb(^{13}C,4n) reaction at 80 MeV with pulsed beams from the ANU 14UD accelerator. Time-correlated γ-γ coincidence spectroscopy performed with the CAESAR detector array has revealed two new isomers above the previously known $17/2^-$, $\tau = 3$ ms isomer. The isomeric states are at $23/2^+$ (2609 keV) and $33/2^+$ (4047 keV) and have lifetimes of 24.6(5) and 53.9(16) ns, respectively. Both configurations involve excitation of an $h_{9/2}$ proton into the $i_{13/2}$ orbital.

Studying the decay from these new isomeric states gave detailed information about previously unknown transitions and states and allowed the construction of the nuclear level scheme for ^{213}Ra to high spin. By measuring the angular distribution of emitted radiation and inferring internal conversion coefficients through the intensity balance of γ decay, spins and parities of newly discovered high-spin states could be firmly identified. The configurations of the newly classified states have been assigned using semi-empirical shell model calculations and are compared with the closed neutron shell neighbour ^{214}Ra and, the systematic behavior of the N = 125 isotones and their relationship to the N = 126 semi-magic neighbours is also discussed.

Contents

List of Figures

List of Tables

Chapter 1
Introduction and background theory

Throughout history, ideas about the shape and composition of the atom have changed dramatically. What started with Democritus [Fur87] and later Dalton's thoughts of indivisibly small particles [Tha66], eventually developed into J.J. Thomson's "Plum Pudding Model" [Tho04] after the discovery of the electron. Through the efforts of Becquerel, Curie and Rutherford, amongst others, the field of nuclear physics was born [Mar06]. Models shifted away from puddings and towards Bohr's positively charged spheres surrounded by clouds of negatively charged electrons. Today, continuing in similar strides, ever more complicated and accurate quantum mechanical pictures of the atom and subatomic structure have been developed.

This thesis will focus on a model where the structure of the nucleus can be explained through the interactions of a few particles moving in orbits outside an inert core. Such a shell structure is in many ways analogous to atomic models of electron clouds, where electrons fill well-defined orbitals with particular energy and angular momentum. In the atomic model, the governing forces are electromagnetic interactions, whereas in the nuclear model interactions are complicated by the inclusion of the strong nuclear force and its smaller (finite) interaction range between particles.

Investigation of nuclei, and the testing of nuclear models, often relies heavily on the measurement and observation of the γ-rays emitted as the nucleus transitions between excited states. This thesis will outline the key aspects of theory relevant to the nuclear shell model, and apply time correlated γ-ray spectroscopy to examine the

shell-model nucleus ^{213}Ra. The results of experiments undertaken in April 2015 will be presented and comparisons of the observed nuclear structure to theoretical shell-model predictions will be discussed.

1.1 Introduction to the shell model

The development of the nuclear shell model derives from the experimental observation of *magic numbers*. When the number of protons or neutrons is one of the magic numbers, the nucleus is observed to be considerably more stable. Specifically, "magic" nuclei exhibit greater total binding energy, larger energies required to separate individual nucleons, higher energy first-excited states and a significantly larger number of stable isotopes and isotones. Magic numbers correspond to closed shells and occur experimentally when either N or Z are equal to 2, 8, 20, 50, 82 and N = 126. While higher closed shells are predicted at Z = 114 and N = 184 [Gre96], they have not yet been observed.

The shell model treats the nuclei with magic numbers as being inert cores, explaining the structure of excited states via the coupling of valence nucleons to the core configuration. Valence nucleons occupy orbitals analogous to the Atomic Shell Model for electrons, where filled electron shells correspond to the noble gases. The orbital occupied determines the angular momentum and parity available to each nucleon. Nucleons can be excited into and out of shells to give rise to higher energy excited states. Considering the interaction of only valence nucleons vastly simplifies theoretical pictures, allowing the prediction of excited state energies, spins and parities for heavy nuclei (near closed shells) without becoming computationally prohibitive.

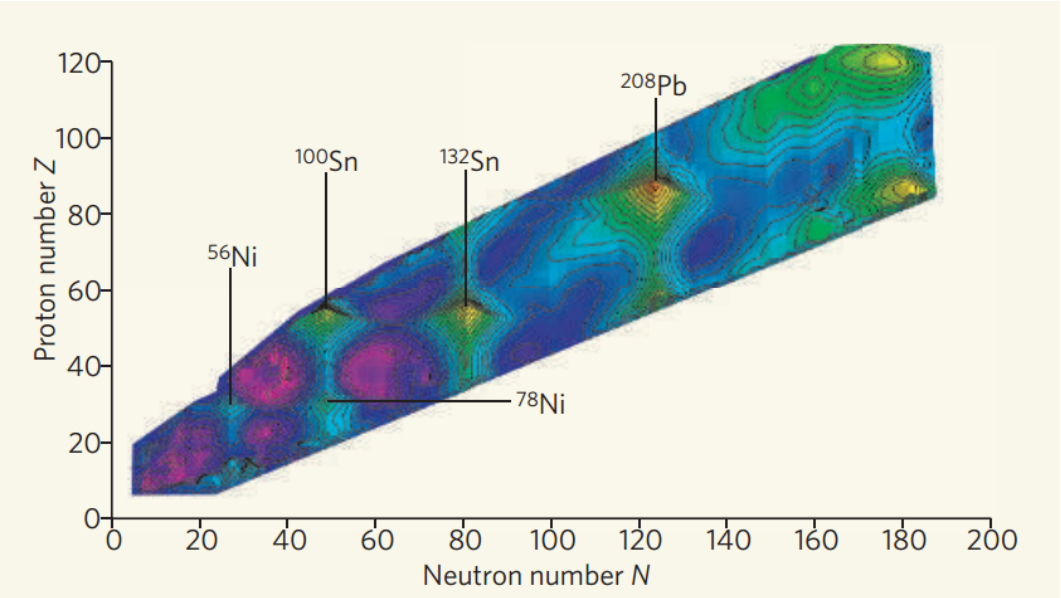

Figure 1.1: The islands of stability. The colour spectrum from violet to red indicates the changing binding energy from less to more bound. The magic numbers at, for example, 28, 50, 82, 126 are evidenced by the ridges and islands at specific nucleon numbers. Picture taken from Ref. [RB07].

1.2 Angular momentum coupling

The angular momentum[1] of valence nucleons can align with each other, adding as vectors, to produce the observed spin of the excited states (Figure 1.2). In the case of ^{210}Po (partial level scheme shown in Figure 1.3) the 0^+ ground state is produced through one $h_{9/2}$ proton contributing $J = 9/2$ and the other producing $J = -9/2$, aligning anti-parallel to each other[2]. This two proton configuration produces states up to a spin and parity of 8^+, while the subsequent states are produced through the excitation of protons into the $f_{7/2}$ and $i_{13/2}$ orbitals. Since protons are fermions, they obey the Pauli exclusion principle, meaning two protons cannot have identical sets of quantum numbers. Therefore the spin of 8^+ state is produced through the protons contributing J = 9/2 and J = 7/2 each. Lower spin couplings are generally energetically favoured, and multiple states of the same spin and parity can exist, each corresponding to a different configuration of valence nucleons, for instance, the

[1]'Spin' and 'angular momentum' are often used interchangeably in nuclear physics. When spin is used to describe a valence particle it is not the intrinsic fermion spin but the total angular momentum of the particle given by $J = l + s$ where l is the orbital angular momentum and s is the intrinsic spin.

[2]This argument is schematic. A rigorous derivation involves the enumeration of m sub-states subject to the Pauli Principle.

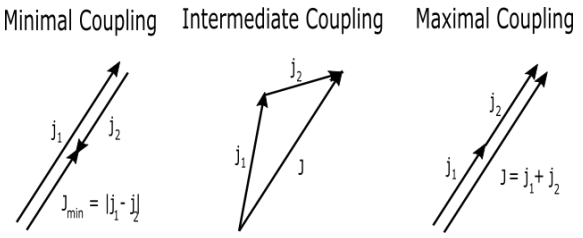

Figure 1.2: The spins of valence nucleons can be treated as vectors added together to produce the net spin of an excited state. As nucleons are fermions the Pauli principle prevents them from having identical sets of quantum numbers.

higher energy 8^+ state in ^{210}Po is produced through the excitation of a $h_{9/2}$ proton into the $f_{7/2}$ orbital.

1.3 Semi-empirical shell model calculations

The inert nature of closed-shell configurations means shell model approaches to theoretical calculations have been developed that consider the interaction of the valence nucleons with each other and the spherical core. Taking this approach allows the energy of states to be expressed in terms of a sum over valence nucleons:

$$E = \sum_{ij} \langle i|V_{ij}|j\rangle + \sum_{i} \langle i|H_{0,i}|i\rangle \tag{1.1}$$

where V_{ij} enumerates the two-body residual interactions and $H_{0,i}$ describes the independent motion of the i^{th} valence nucleon in an average potential well, which can be written [Law80]:

$$H_{0,i} = \frac{p_i^2}{2m} + V_1(r_i) + V_2(r_i, p_i)\tilde{\sigma_i} \cdot \tilde{l_i} \tag{1.2}$$

In Equation 1.2 V_2 is generally an attractive potential and $\frac{p_i^2}{2m}$ defines the kinetic energy of the i^{th} nucleon. An appropriate choice of the potential V_1 is the Woods-Saxon potential which is strongly attractive within the nucleus and rapidly goes to zero outside the nuclear radius [Kra87]. It is defined by

$$V(r_i) = \frac{-V_0}{1 + exp[(r_i - R)/a]} \tag{1.3}$$

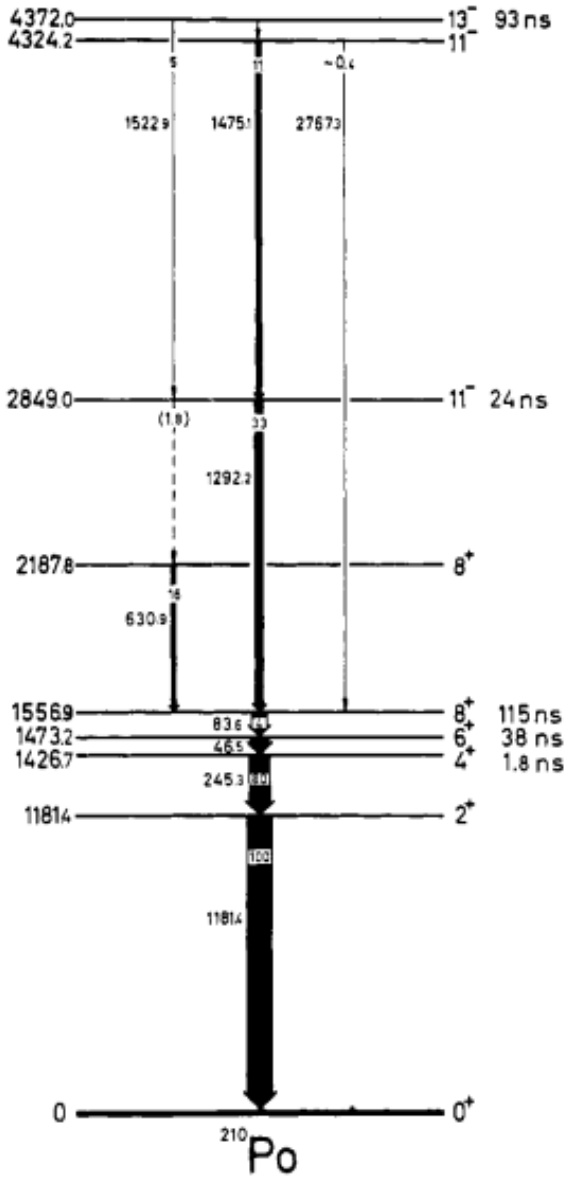

Figure 1.3: Partial level scheme of ^{210}Po [Blo71]. The spin and parity of the 2^+, 4^+, 6^+ and 8^+ states results from the coupling of two $h_{9/2}$ protons outside doubly-magic ^{208}Pb.

where a and R give, respectively, the skin thickness and mean radius of the nucleus. V_0 defines the depth of the well, typically on the order of 50 MeV [Woo54, Kra87]. The addition of the spin orbit term $(\tilde{\sigma_i} \cdot \tilde{l_i})$ is necessary to successfully reproduce the closed shell magic numbers shown in Figure 1.4 [May50a, May50b]. This accomplishment which led to Eugene Paul Wigner, Maria Goeppert Mayer and J. Hans D. Jenson sharing the 1963 Nobel prize. Rather than direct calculation, the semi-empirical shell model defines the matrix elements in Equation 1.1 from experimental energy levels, as will be described below.

1.3.1 Single particle interactions

The single particle potential is the same for every nucleon occupying a particular orbital. To determine the single particle excitation energies ($\langle i|H_{0,i}|i\rangle$) for all nuclei in the trans-lead region, only four different cases need to be known as these numbers can then be extended to every nucleus near the closed ^{208}Pb shell. These cases are: the valence proton (π) energies given by excited states in ^{209}Bi, the valence neutrons (ν) from ^{209}Pb, the valence neutron holes (ν^{-1}) from ^{207}Pb and the valence proton holes (π^{-1}) from ^{207}Tl. The value of the single-particle excitation energy is therefore taken as the difference in binding energy between ^{208}Pb and the excited state of the relevant nucleus with an added or removed nucleon. Figure 1.5 shows the single particle energies relative to ^{208}Pb for various orbitals in the four nuclei mentioned above. Binding energies are taken from the Audi and Wapstra tables [Aud03].

1.3.2 Two-body residual interactions

Recoupling two valence particles to different angular momentum understandably results in a different energy to the single particle case as these particles will also be interacting with each other. The effect of the interaction can be determined experimentally, again in relation to the ^{208}Pb core. Figure 1.6 shows the two-body residual interaction of two $h_{9/2}$ protons coupling to different states in ^{210}Po along with the predicted ground state using only the single particle potential. It can be seen that the 0^+ coupling is especially favoured, 2^+ slightly favoured, while the 4^+ coupling actually increases the energy.

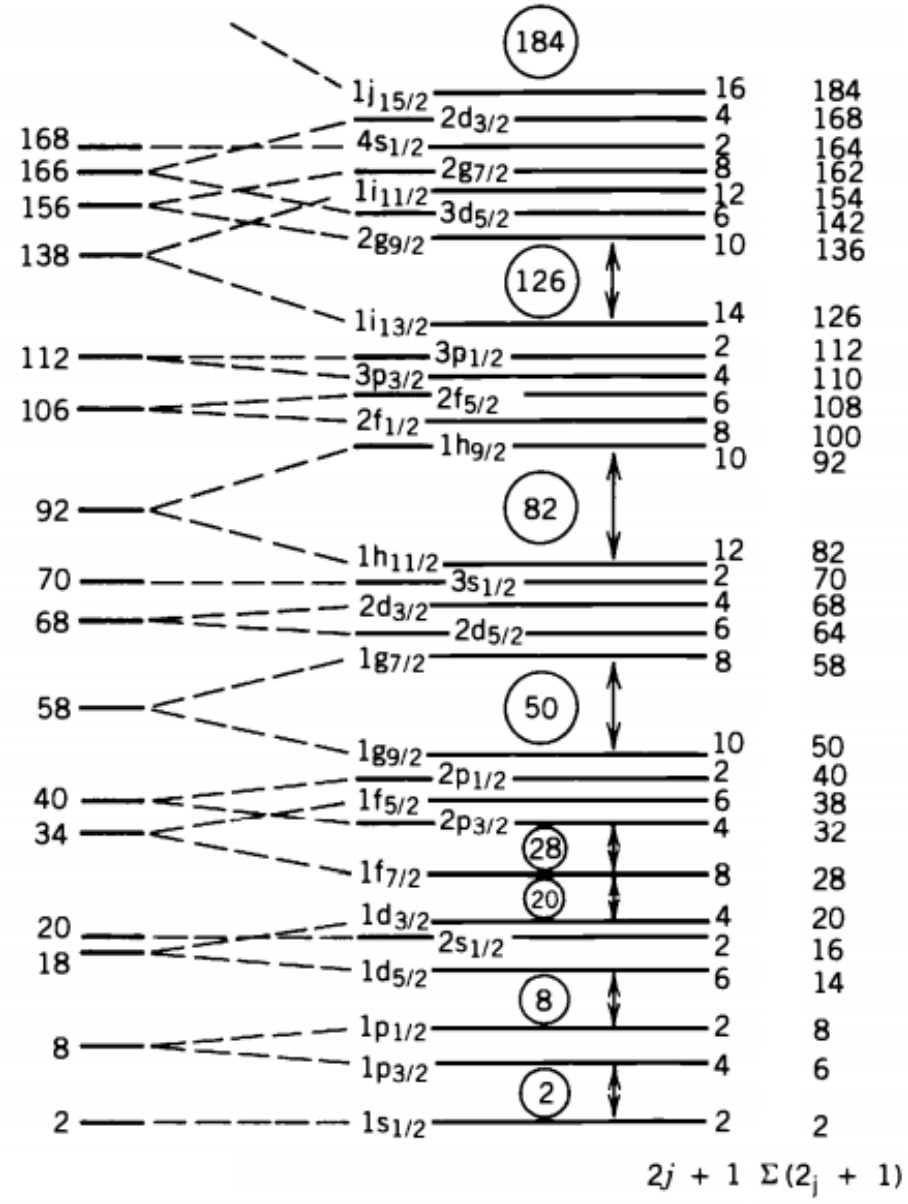

Figure 1.4: The closed shell predictions of the shell model. Each level with angular momentum J can contain 2J + 1 particles [Kra87]. The parity of the state is given by the orbitals occupied by the valence nucleons. The orbitals; s, p, d, f, g (and so on alphabetically) have alternating parity starting with positive parity on the s orbital.

As with the single-particle case, two-body residual interactions do not need to be known for every nucleus, only for the different combinations of interactions between two nucleons adjacent to ^{208}Pb. For example, ^{210}Po gives the two-body interaction for π-π, ^{206}Pb gives ν^{-1}-ν^{-1} and ^{210}Bi gives $\pi - \nu$. Most two-body residual interactions have been directly observed, however, these generally correspond to lower-lying excitations. Higher excited configurations do surely exist but the fact that they have not been observed indicates that their contribution may be less rel-

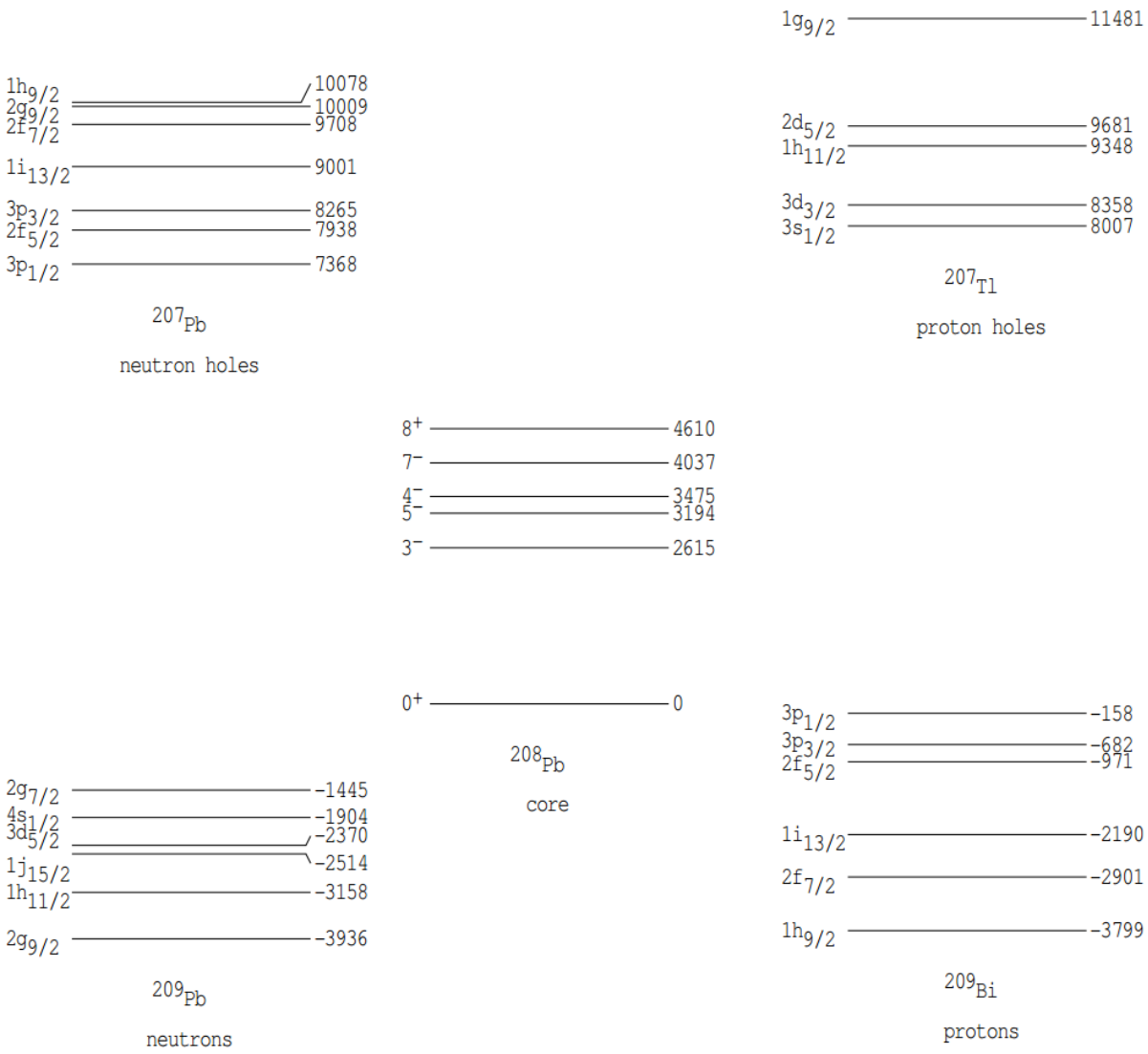

Figure 1.5: Experimentally measured single particle energies (in keV) for orbitals near doubly-magic ^{208}Pb. Figure from [Byr86]

evant. In the present work, theoretical values are used if empirical energies are not available.

A convenient way of representing these multi-particle interactions was developed by MacFarlane and French [MacF 60]. It involves decomposing the wave functions of the total system into the wave functions for each of the valence nucleons. It is a diagrammatic approach (illustrated in Figure 1.7) which reduces the total interaction to a sum over all possible two-body interactions, and in which triangles represent the vector-coupling of angular momentum. These contributions are weighted, and the weights come from angular momentum algebra. The details of this process are beyond the scope of this project; fortunately computer code written by A. E.

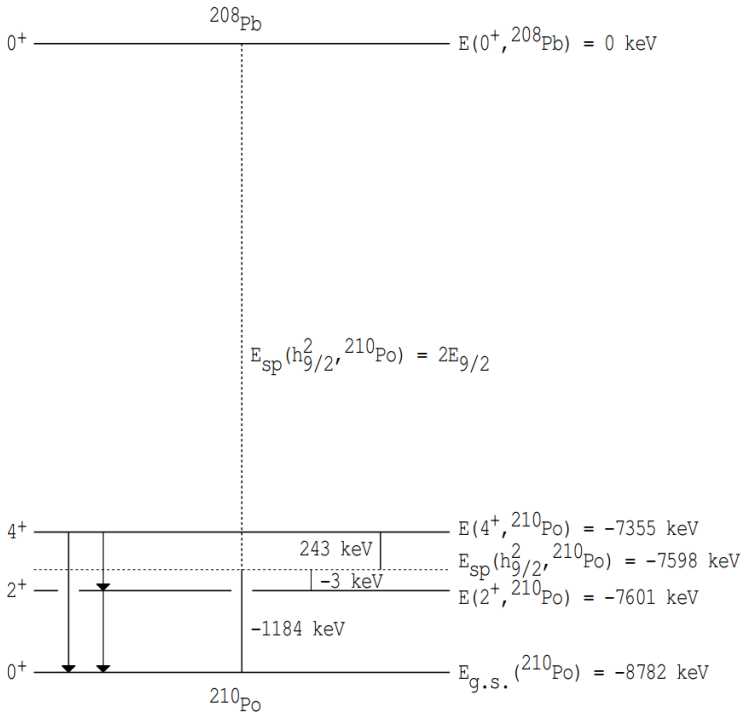

Figure 1.6: Two body interactions of the $h_{9/2}$ protons deduced from excited states in ^{210}Po. The energy of the residual interactions is shown for the 0^+, 2^+ and 4^+ states. The dotted line represents the ground state energy of ^{210}Po relative to ^{208}Pb assuming two non-interacting protons. The solid lines are the observed states and the total energy is with respect to ^{208}Pb. [Mar12]

Stuchbery [Stu15] performs it automatically.

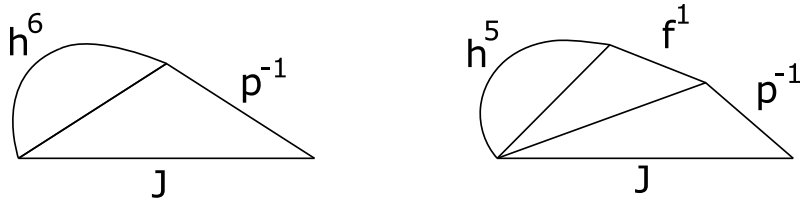

Figure 1.7: At left: The interaction of six $h_{9/2}$ protons and one $p_{1/2}$ neutron hole to produce the total spin. At right: the interaction of five $h_{9/2}$ protons, one $f_{7/2}$ proton and one $p_{1/2}$ neutron hole.

1.4 Selection rules

Transitions between excited states in the nucleus can proceed via the emission of electromagnetic radiation. Such transitions have a multipolarity denoted XL, where X defines whether the transition is electric or magnetic in nature and L is the angular momentum (in units of $\hbar$) carried by the field. Each nuclear state is defined by its spin J_i, and parity π_i. The γ-ray transitions between states must therefore conserve the total angular momentum such that:

$$\hat{J}_i \;=\; \hat{J}_f + \hat{L} \tag{1.4}$$

where the subscripts i and f refer to the initial and final states and $\hat{J}_i$, $\hat{J}_f$ and $\hat{L}$ are the angular momentum vectors. Hence, selection rules dictate the allowed kind of radiation emitted in the depopulation of an excited state. The allowed multipolarity of a γ transition is given by:

$$|\hat{J}_i - \hat{J}_f| \;\leq \hat{L} \leq \hat{J}_i + \hat{J}_f \tag{1.5}$$

Transitions can therefore consist of a mixture of multipolarity transitions where the lowest permitted multipolarity transition is generally favoured [Mor76]. Because photons must carry intrinsic angular momentum of at least $1\hbar$, monopole (L = 0) photon transitions are strictly prohibited. In general, low multipolarity transitions are more competitive than high multipolarity transitions, however, since electric transitions are more probable than magnetic transitions, mixed Mλ/E(λ + 1) transitions are possible. Thus, for example, an E2 will often compete with an M1. The degree of competition is defined by the mixing ratio (see Section 2.4). Parity conservation also necessitates parity selection rules, these are

$\pi_i = \pi_f$ for electric transitions with even L and magnetic transitions with odd L
$\pi_i \neq \pi_f$ for electric transitions with odd L and magnetic transitions with even L

These rules give rise to the concept of *forbidden transitions*. The term forbidden does not always mean the transition is not possible. Rather, it means the transition is hindered in decay rate. A J-forbidden transition occurs when

the change in particle configuration (from one orbital to another) is greater than the angular momentum carried by the photon, remembering that total angular momentum is still conserved through recoupling the nucleon's angular momenta. An example of this is in ^{204}At. The transition from the isomeric 10^- state to the 7^+ state carries angular momentum $3\hbar$ (an E3 transition). However, the particle configuration involves the change of an $i_{13/2}$ neutron to an $f_{5/2}$ neutron i.e $\Delta J = 4\hbar$, thus the transition is J-forbidden [Gip75].

Forbidden transitions increase the lifetime of a state as well as affecting the ability of the specific decay to compete with other transitions leaving the same state.

1.5 Weisskopf estimates

The decay rate (λ) of a state is intrinsically linked to the nature of the decays depopulating it[3]. Higher multipolarity transitions will tend to exhibit slower decay rates and forbidden transitions slow depopulation even further. Weisskopf estimates are nominal rates for single particle transitions; they thus provide a convenient scale for the decay rate of states.

Decay rates are often expressed in Weisskopf units (W.u), defined by $\frac{measured\ rate}{Weisskopf\ rate}$, hence giving an indication of the strength relative to a typical single-particle transition. The Weisskopf decay rate is derived by assuming the electromagnetic transitions are caused by the change of a single nucleon from one "generic" orbital to another [Gre96]. Table 1.1 shows the Weisskopf γ-ray transition rate as a function of mass and energy (MeV) for different multipolarities. In this work, measured transition rates will be compared to Weisskopf estimates as secondary evidence for justifying the spin and parity assignments presented in Chapter 3.

For states with multiple competing transitions, the following equation can be used to determine the transition rate of each γ-ray.

$$\lambda_\gamma(XL) = \frac{N_\gamma(XL)}{\sum_d N_d}\frac{1}{\tau} \tag{1.6}$$

Where $\lambda_\gamma(XL)$ is the partial γ-ray transition rate, $N_\gamma(XL)$ is the γ-ray intensity,

[3]The lifetime of a state, τ, is $\frac{1}{\lambda}$

Table 1.1: Weisskopf decay rates for different multipolarity transitions. A is the atomic mass and E is the transition energy in MeV [Kra87].

Multipole	Electric	Magnetic
1	$1.025 \times 10^{14} A^{2/3} E^3$	$3.145 \times 10^{13} E^3$
2	$7.279 \times 10^{7} A^{4/3} E^5$	$2.236 \times 10^{7} A^{2/3} E^5$
3	$33.91 A^2 E^7$	$10.42 A^{4/3} E^7$
4	$1.067 \times 10^{-5} A^{8/3} E^9$	$3.278 \times 10^{-6} A^2 E^9$

$\sum_d N_d$ is the total γ-ray intensity of transitions depopulating the state and τ is the lifetime of the state. To obtain the total transition decay rate we sum the partial γ-ray decay rates:

$$P_T = \sum_i (\lambda_{\gamma_i} + \lambda_{IC_i}) \tag{1.7}$$

λ_{IC} is the transition probability due to internal conversion (discussed in Section 2.5). Figure 1.8 shows the Weisskopf estimates of the partial γ-ray lifetime as a function of energy for ^{213}Ra for different multipolarity transitions depopulating it.

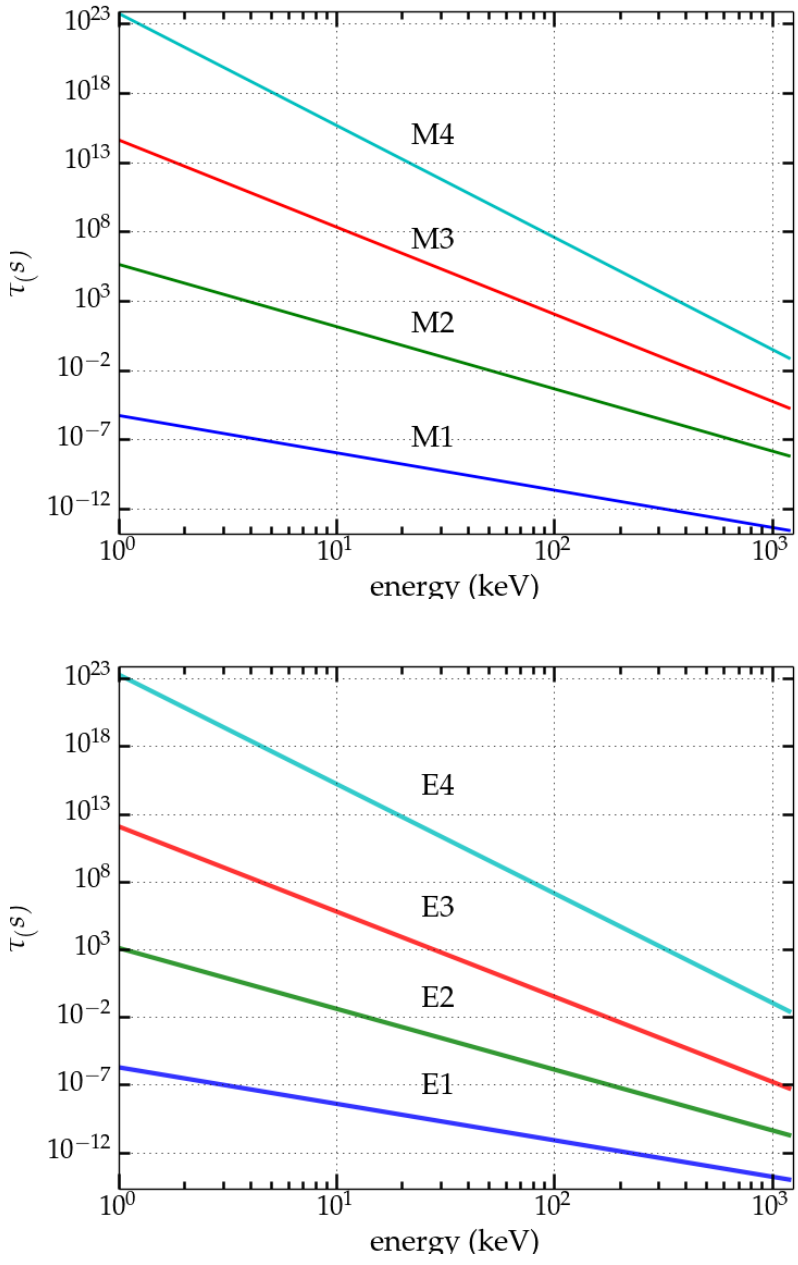

Figure 1.8: The partial γ-ray lifetime as a function of the energy for magnetic and electric transitions calculated using Weisskopf estimates.

1.6 The case of ^{213}Ra

Nuclei in the region around doubly-magic ^{208}Pb are well known as a testing ground for the nuclear shell model. Nuclei in this region often have long-lived isomers (states with measurable lifetimes) formed from simple particle configurations that have their component nucleon angular momenta fully aligned to the maximum possible value. The 8^+ isomer in ^{210}Po is, for instance, produced by the maximal coupling of the two $h_{9/2}$ protons and is isomeric due to the low energy decay to the 6^+ state of the same configuration.

While many nuclei in this region are well studied, there are a number of neutron-deficient cases where fission competition complicates production of the excited nucleus, or where a very long-lived isomer has precluded simple correlations of the high-spin level scheme with the known low-lying states. The subject of the present work, ^{213}Ra, is one such case.

^{213}Ra has six valence protons and one neutron hole outside of the ^{208}Pb core; the ground state configuration is therefore given by the six $h_{9/2}$ protons coupling to zero and the $p_{1/2}$ neutron contributing 1/2, leading to a $1/2^-$ ground state. Such configurations will be written as $(\pi h_{9/2})^6_0 \otimes (\nu p_{1/2})^{-1}_{1/2}$; similar forms will be used throughout this work[4]. Current knowledge of ^{213}Ra is limited to excited states up to the $17/2^-$ ($(\pi h_{9/2})^6_8 \otimes (\nu p_{1/2})^{-1}_{1/2}$), $\tau = 3$ ms, isomeric state [He04]. Several neighboring radium isotopes have been studied to high spin including the closed neutron shell nucleus ^{214}Ra. While every nucleus is unique, similarities in excited states will arise between ^{213}Ra and ^{214}Ra as there is only the additional coupling of a $p_{1/2}$ neutron hole in ^{213}Ra. Arguments of this nature will be used to help understand the structure of the ^{213}Ra states that have been newly observed as part of this work.

[4]The superscript on the configurations denote the number of particles in this orbital. The subscript is the spin value they couple to.

Chapter 2
Experimental Methods

In the nucleus, transitions between excited states, and the release of the energy lost, can occur in two principle ways, the excitation and emission of an atomic electron (internal conversion) or the emission of a γ-ray. The latter process can be exploited using time correlated γ-ray spectroscopy to derive the nuclear level scheme by detecting the de-excitation of the nucleus. Photons emitted in a transition between excited states carry discrete energy and also have an associated spin and parity. Measuring these properties gives information about the relationship between parent and daughter states in the transition. Time correlated γ-ray spectroscopy provides a means of measuring these properties by detecting the γ-rays emitted during de-excitation, the time between successive decays, and the angular distribution of emitted photons. The methods of time correlated γ-ray spectroscopy will be described in this chapter.

2.1 CAESAR

CAESAR is the primary detector system at the ANU for time-correlated γ-ray spectroscopy. It features nine Compton suppressed high-purity germanium (HPGe) semi-conductor detectors and two low-energy photon spectrometers (LEPS). After the completion of this work, as part of another students honours thesis, 6 additional LaBr detectors have been added to give additional lifetime measurement capabilities. The typical operating efficiency of the array is on the order of 1%, comparable to the solid angle covered by the detectors.

Six of the HPGe detectors are aligned in the vertical plane of the beam line forming

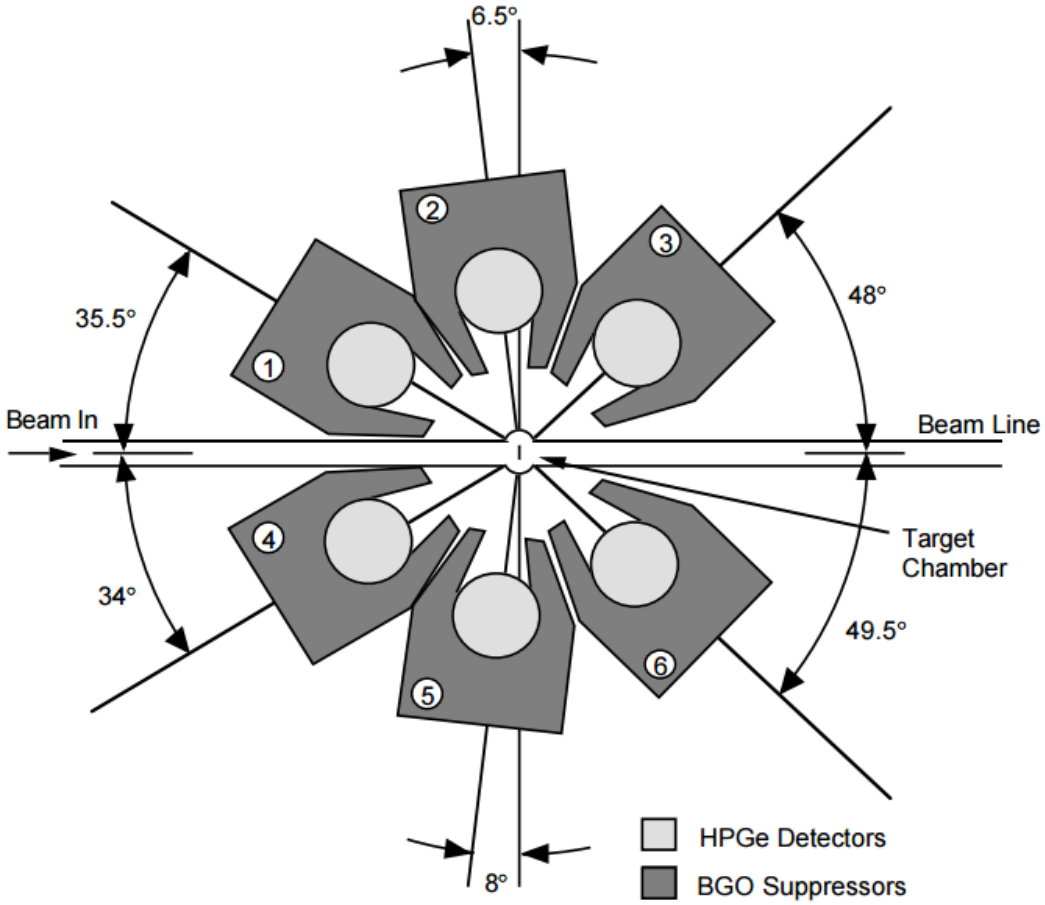

Figure 2.1: Schematic diagram of the CAESAR array. The LEPS and remaining HPGe detectors are 90° out of the page. Figure taken from Ref. [Lan95]

three pairs of angles, as shown in Fig. 2.1, in order to measure the angular distribution of emitted radiation relative to the beam axis. The other three detectors are out of the vertical plane angled at approximately 49°, 53° and 132° with respect to the downstream beam axis. The two LEPS detectors give the array the ability to detect and resolve low energy lines. Additionally, their lifetime measurement capability is better than the HPGe detectors for low energy transitions. Unfortunately, due to an oversight after an unscheduled power outage, Compton suppression was not active during the experiment, resulting in a greater than usual continuous background in the γ-ray spectra.

2.1.1 Coincidence measurements

The decay of a nucleus from one excited state to another proceeds through the emission of a γ-ray. Recording purely the decay gives an indication of the radiation emitted during the experiment but reveals few details about the level scheme of the nucleus. It is often more useful to consider *coincidence events* rather than just the observation of single photons. A coincidence event requires that two γ-rays are detected within a specified time (ΔT) of each other for it to be recorded as a valid event. Beyond recording the energy and general coincidence relationships, this method of data collection also allows the inference of nuclear lifetimes, if the time difference between the arrival of two γ-rays or with respect to a pulsed beam is also recorded.

The ANU 14UD heavy-ion accelerator is capable of providing beam pulses that are less than 1 ns wide and integer multiples of 107 ns apart. Signals derived from the beam pulsing are used as a natural reference for measuring γ-ray arrival times. This experiment, for instance, used 1712 ns beam pulsing and a maximum coincidence overlap between two γ-rays of ΔT = $\pm$856 ns. The γ-rays detected outside this window will not be registered as being coincident with each other. This is a powerful tool as one can choose to select data which arrive after or during a specific time interval. By selecting longer time differences between detection events, decay from short-lived states can be filtered out, however, random contaminant coincidences are enhanced. Conversely, selecting shorter time intervals allows the viewing of 'prompt' decay from short-lived states while reducing random coincidences. A convenient way of sorting data for off-line analysis is discussed in the next section.

2.2 Sorting of data and construction of matrices

Data analysis can be greatly simplified by sorting events into coincidence matrices. A matrix records the number of decays observed by the detectors as a function of energy with events sorted into many different kinds of matrices with different time-correlated pairs of γ-rays on each axis. Matrices can contain different classes of events, for example:

- short or long-lived decay by gating on different time regions after the beam pulse,
- the intensity of radiation as a function of angle of emission, by sorting only particular detection angles on one axis, or
- the coincidences between HPGe and LEPS detectors to better resolve low-energy features by sorting HPGe detectors onto one axis and the LEPS detectors onto the other.

Decay events are represented in a multi-dimensional, γ-time space. The γ axes are the energies of coincident γ-rays and the time axis can be either the time difference between γ-rays *or* the absolute times of arrival for the γ-rays relative to the beam burst. By selecting different time-cuts, data can be sorted into: short, long, narrow, wide, in-beam, out-of-beam and early-delayed matrices. Early-delayed matrices reveal transitions from isomeric states by showing events early with respect to the gated (delayed) transition allowing one to determine the order of the γ-rays in the level scheme. The nomenclature and specific time cuts are shown in Table 2.1 and Figure 2.3.

The bulk of the analysis involves examination of these two-dimensional coincidence matrices. 'Gating' is done on particular gamma-ray peaks, or regions, to project the γ-rays coincident with that peak. Using a variety of coincidence information, the precise order and location of transitions in the level scheme can be determined. An example of this is shown in Figure 2.2 below.

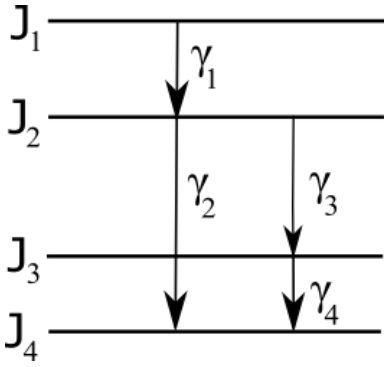

Figure 2.2: By recording coincidence events the nuclear level scheme can be constructed. In this example level scheme γ_1 will be recorded in coincidence with γ_2, γ_3 and γ_4. Similarly, γ_3 and γ_4 will also be in coincidence with each other as they are in the same cascade, however, γ_2 will not be coincident with either γ_3 or γ_4 as they form a parallel decay path from the state J_2

Table 2.1: Time conditions used to sort data into matrices in the present work.

Matrix name	Absolute time T_{γ_1}	T_{γ_2}	Time diff ΔT (ns)
prompt narrow	-25→+30	-25→+30	-30 → +30
prompt wide (p. w.)	-25→+150	-25→+150	-150 → +150
narrow	-25→+1415	-25→+1415	-30 → +30
wide	-25→+1415	-25→+1415	-150 → +150
out-of-beam short	+30→+150	+30→+150	-150 → +150
out-of-beam long (o. b. l)	+150→+1415	+150→+1415	-150 → +150
early-delayed short	-25→+1415	-25→+1415	+30 → +150
early-delayed long	-25→+1415	-25→+1415	+150 → +856
p. w. - o. b. l.	-25→+150	+150→+1006	-856 → +856

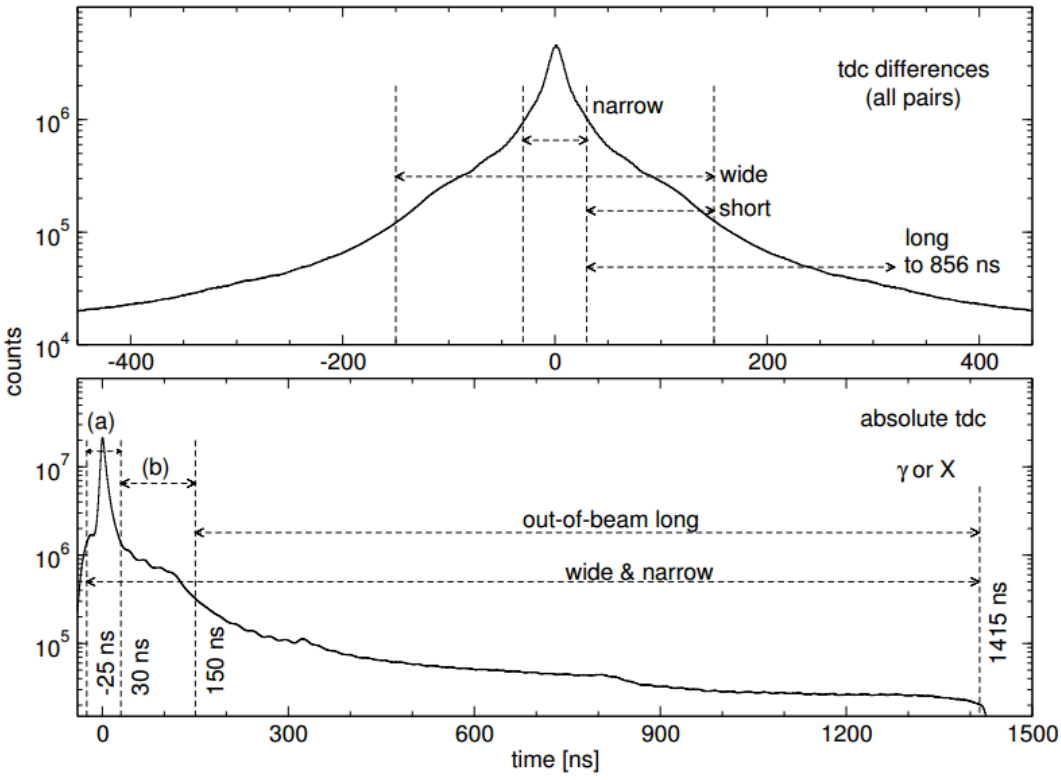

Figure 2.3: Example time cuts used. The upper plot shows the projected γ-γ-ΔT spectra. The lower panel shows the absolute tdc spectrum (a) refers to the prompt-narrow time cut while (b) refers to the out-of-beam short time cut. These different cuts are used to sort decay events into different matrices for data analysis. Figure from Ref. [Mar12]

2.3 Efficiency calibration

The energy efficiency of the detectors in the CAESAR array must be calibrated with respect to reference values [Rad95] before the γ-ray intensities can be determined and used to evaluate angular distributions and internal conversion coefficients. This must be done for *every* experiment as the detectors suffer from neutron damage and general degradation over time, decreasing their energy efficiency, while there are also electronic thresholds that are adjusted, depending on the nature of the experiment, which can also affect efficiency.

At the end of the experiment ^{152}Eu and ^{133}Ba sources were placed in the array and the decay was measured. The efficiency (as a function of energy) is then determined by fitting the intensity of particular decay peaks in the ^{133}Ba and ^{152}Eu spectra and dividing by the reference intensities for those peaks. The energy dependent efficiency curve of CAESAR for this experiment is shown in Fig. 2.4.

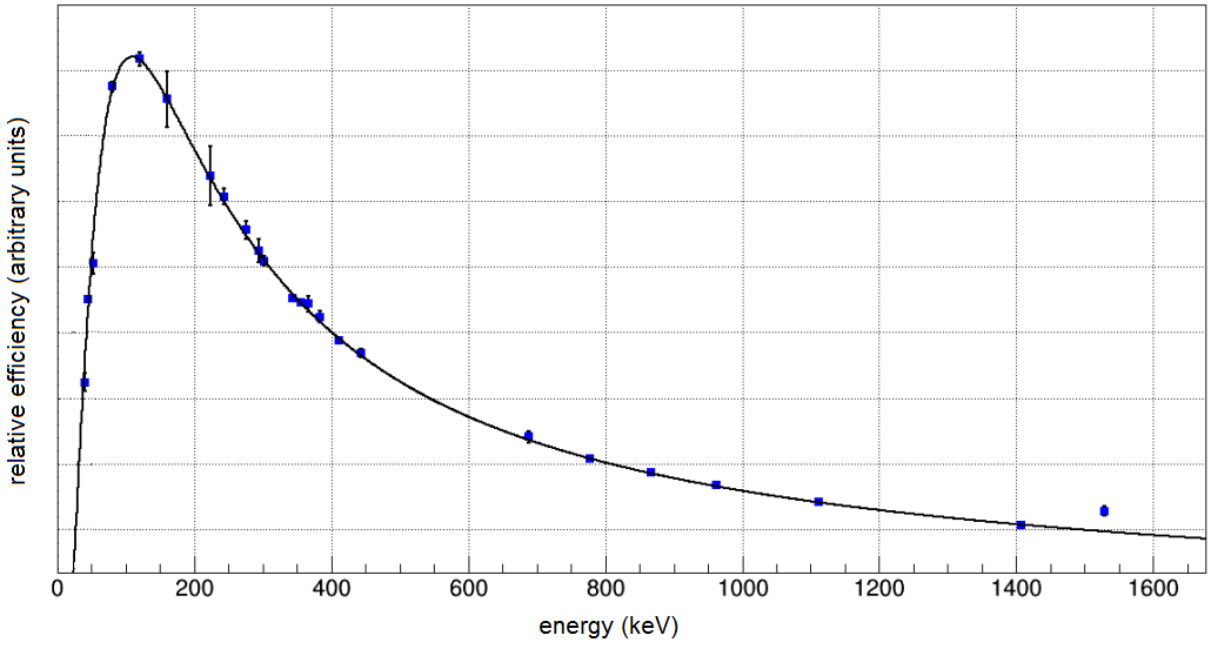

Figure 2.4: Combined efficiency of the 9 HPGe detectors obtained by comparing the observed intensities to known values for ^{133}Ba and ^{152}Eu. This is a relative efficiency curve with the y-axis having arbitrary units

2.4 Angular distributions

Photons emitted in the depopulation of excited states carry discrete angular momentum. The angular pattern of emission intensity depends on the photon angular momentum *and* the direction of the nuclear angular momentum vector. In heavy ion reactions, nuclear angular momentum is aligned in the plane perpendicular to the beam axis as shown in Figure 2.5 below.

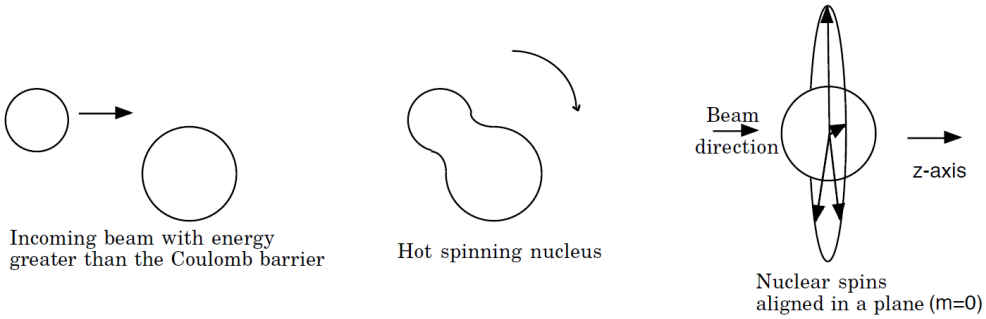

Figure 2.5: Schematic diagram of heavy-ion reactions. After the formation of the nucleus spins align in a plane perpendicular to the beam axis. Figure from Ref. [Mar12].

This drastically simplifies the problem allowing the use of Legendre polynomials to fit the angular intensity distribution of the γ-rays. Since CAESAR detects radiation at three sets of emission angles, only up to the second order (A_2) term can be fitted. The equation for the angular distribution of γ-rays emitted from an oriented source is given below:

$$W(\theta) = A_0 + A_2 P_2(cos\ \theta) \tag{2.1}$$

where A_λ is given in reference [Ste80] as:

$$A_\lambda = \frac{B_\lambda(J_i)}{1+\delta_{12}^2}[F_\lambda(L_1 L_1 I_f I_i) + 2\delta_{12}(\gamma_{12})F_\lambda(L_1 L_2 I_f I_i) + \delta_{12}^2 F_\lambda(L_2 L_2 L I_f I_i)] \tag{2.2}$$

J_i and J_f are the initial and final spins of the states, L is the angular momentum of the transition and F_λ is the generalised F-coefficient (tabulated in Ref. [Mor76]). B_λ is the radiation orientation coefficient defined in [Stu03]:

$$B_\lambda(J_i) = \sqrt{2J_i+1}\ \sum_m (-1)^{J_i+m}\langle J_i - m J_i m|\lambda 0\rangle P_m \tag{2.3}$$

where λ = 0, 1, 2,..., 2J for integer spin and λ = 0, 1, 2,..., 2J-1 for half integer spin.

$P(m)$ is the m substate distribution given by:

$$P_m = \frac{\exp(-m^2/2\sigma^2)}{\sum_{m'=-J_i}^{J_i} \exp(-m'^2/2\sigma^2)} \tag{2.4}$$

σ describes the width of the distribution. In Equation 2.2, δ_{12} is the mixing ratio (as mentioned in Section 1.4) giving the relative transition amplitudes of γ_1 and γ_2 and is defined as follows:

$$\delta_{12} = \frac{I(\gamma_1)}{I(\gamma_2)} \tag{2.5}$$

A mixing ratio of 0 implies a pure transition. The ratio of A2 to A0 gives an indication of the angular momentum of the emitted photon as well as its mixing ratio. Table 2.2 show values associated with pure dipole, quadrupole and octupole transitions.

Table 2.2: Values of A_2/A_0 typical of nuclei in the trans-lead region.

Multipole	L	A_2/A_0
Dipole	1	-0.21
Quadrupole	2	0.28
Octupole	3	0.46

Long-lived isomeric states (lifetimes on the order of hundreds of nanoseconds) cause a loss of spin alignment due to hyperfine interactions[1]. This means transitions from states populated in the decay of an isomer often cannot have their angular distribution measured.

[1]Interactions between the atomic and nuclear spin eventually lead to a random alignment of the nuclear spin. This is a slow process, so it only effects long lived states. [Ste80]

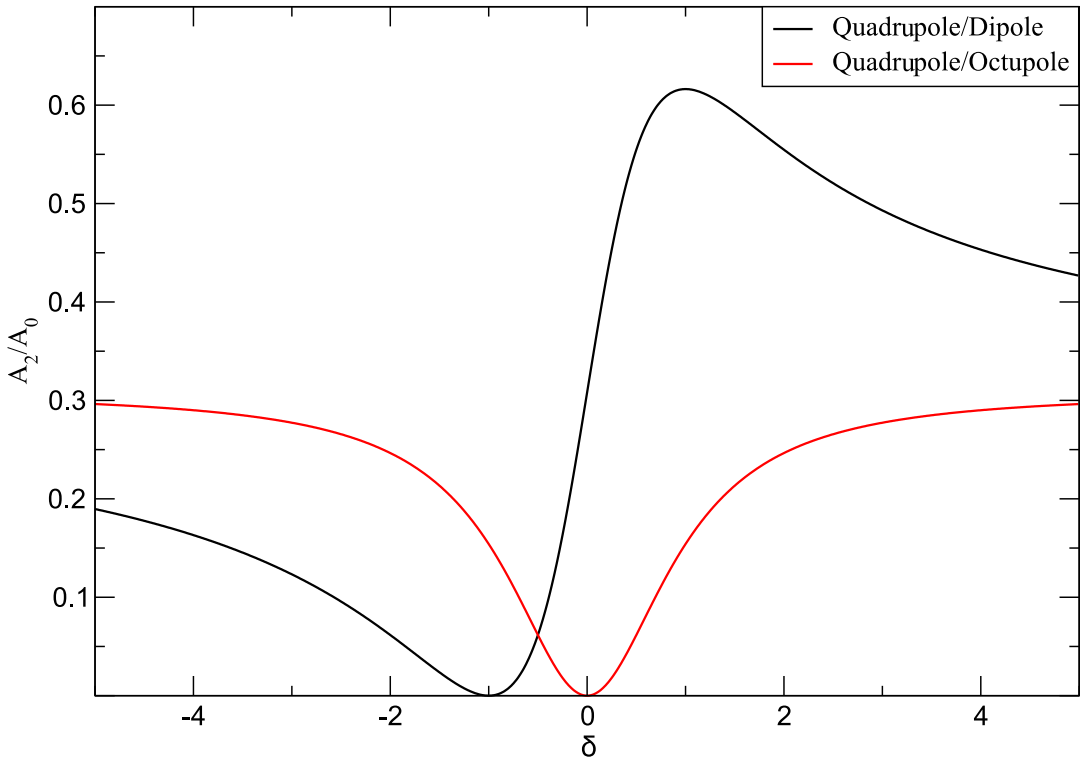

Figure 2.6: Values of $\frac{A_2}{A_0}$ as a function of mixing ratio, δ, for mixed dipole/quadrupole and quadrupole/octupole transitions.

2.5 Internal conversion

Internal conversion is a nuclear transition process where an atomic electron interacts electromagnetically with an excited nucleus and is emitted from the atom. Internal conversion (IC) is not the same as beta decay, as the emitted electron has not been created in the decay process but originates from an orbital electron [Kra87]. Such transitions have a probability relative to photon emission, α_T, and are independent of the γ decay probability, although the electron takes away angular momentum equivalent to the γ decay. There are many ways of determining internal conversion coefficients, this study will focus on one such method: intensity balances. In this method it is assumed that the intensity feeding a state must equal the intensity leaving a state, the total intensity is thus:

$$I_{total} = I_{\gamma}(1 + \alpha_T) \tag{2.6}$$

Where $I_{total} = I_{\gamma} + I_{IC}$ and I_{γ} is the measured γ-ray intensity and $I_{IC} = I_{\gamma} \times \alpha_T$. In Figure 2.2, for example, to determine the internal conversion coefficient of γ_4 one would gate on γ_1 and measure the intensity of the transitions γ_3 and γ_4. The following equation can then be used to calculate the internal conversion coefficient:

$$1 \ + \ \alpha_{T_{\gamma_4}} = \frac{I_{total_{\gamma_3}}}{I_{\gamma_4}} \tag{2.7}$$

$I_{total_{\gamma_3}}$ can be set equal to $I_{total_{\gamma_4}}$ because of the assumption that the total intensity feeding a state equals the total intensity leaving a state.

2.6 Lifetime measurements

Long-lived isomeric states are highly sought after in time correlated γ-ray spectroscopy. They provide important structural information about the nucleus as they probe the overlap between the wave functions of the parent and daughter states, for example, exposing forbidden transitions or when the angular momenta of valence nucleons are aligned to produce maximal coupling. Isomers can provide the key arguments for the assignment of configurations both to the state in question and

those populated in its decay. Consequently they are an important area of study.

In this work, lifetimes of states have been determined by creating γ-γ-ΔT cubes, where the time axis is the time difference between the arrival of the two γ-rays[2] Lifetimes are determined by gating on the two γ axes and projecting the time-difference spectrum, referred to as a (γ_1, γ_2) slice. If γ_1 is above an isomer and γ_2 below, the projected time spectrum will show a positive time difference and vice-versa for the (γ_2, γ_1) slice.

The projected slice is a histogram of time differences, i.e the number of times the state took to decay for each value of time difference. This histogram is fitted with the *prompt response function* (typically a Gaussian) to describe the timing response of the detector. The prompt response function is convoluted with a decaying exponential. The gradient of the exponential decay term (when plotted on a logarithmic scale) gives the lifetime of the state. Using this technique the CAESAR array is capable of resolving mean-lives as low as 0.5ns in the case of favourable statistics. By way of example, the lifetime curve obtained for the 10^- state in ^{210}Fr by Margerin *et al* [Mar12] is shown in Fig. 2.7. Generally, the prompt response and time walk of detectors is worse at lower energies[3].

[2]They can, alternatively, be made with respect to beam pulsing, this instead produces a γ-tdc curve.

[3]Time walk is the stretching of time difference signals, resulting in decay being present in longer time-cut matrices than the true lifetime of the transition would allow. It is due to a combination of factors (such as non-uniform electric fields in the detectors and different γ-ray interaction positions in the detector crystal) but is most prevalent for low energy photons.

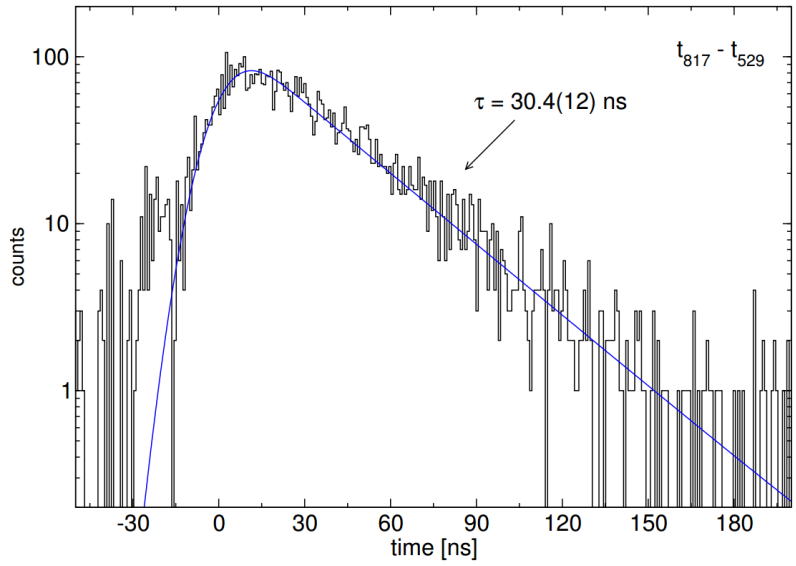

Figure 2.7: Time difference between the 817 keV and 529 keV transitions giving the lifetime of the 10^- state in ^{210}Fr. Figure from Ref. [Mar12].

Chapter 3
Analysis and Results

Neutron-deficient heavy nuclei are often difficult to study due to high rates of fission in heavy-ion reactions. Hence, although ^{213}Ra was the subject of three previous studies, none of them populated the nucleus to high spin. The α-decay studies of ^{213}Ra by D. Raich *et al* identified excited states up to the isomeric, τ = 3ms, $17/2^-$ state [Rai76]. Subsequent studies of ^{213}Ra by Rassmussen *et al* suggested the existence of a $\Delta < 1$ keV transition between the $17/2^-$ and $13/2^-$ states on the basis of α-decay rate calculations [Ras76] though this fact was only confirmed 18 years later in 1994 with g-factor measurements by G. Neyens *et al* [Ney94]. The level scheme that was known prior to the present high spin studies of ^{213}Ra undertaken is shown below. There is, however, disagreement as to whether the E4 transition

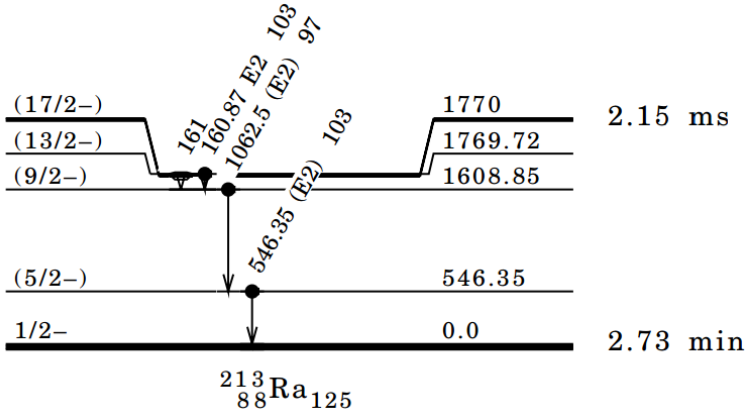

Figure 3.1: Level scheme for ^{213}Ra prior to this work. It should be noted that half lives are given above rather than mean lives. [Bas07]

from the $17/2^-$ to $9/2^-$ state observed previously exists. Data collected during this experiment shows no evidence of this transition and a 161 keV E4 transition

would typically exhibit a lifetime of days, not milliseconds (as shown in Section 1.5). Consequently it has not been included in the new level scheme for ^{213}Ra deduced from present work shown in Fig. 3.2.

High spin states in ^{213}Ra were populated by bombarding a pure ^{204}Pb target (enriched to greater than 99%) with a beam of ^{13}C ions initially at 75 MeV. The beam energy was increased to 80 MeV after 24 hours in order to excite the nucleus to higher spin and obtain a higher reaction yield of ^{213}Ra. A pulsed beam with 1 ns on and 1712 ns off was used to isolate and resolve the decays of short isomeric states. After 3 days, the beam was changed to long chopping, with 1 ms on and 3 ms off, to search for other long-lived isomers and to enable the subtraction of long-lived contaminants from the spectra of interest.

This chapter presents results from the experimental measurements conducted during this work. The determination of the level scheme of ^{213}Ra through time-correlated γ-ray spectroscopy is discussed in Sections 3.2 and 3.2, while discussions of lifetime measurements and spin and parity assignments are presented in Sections 3.3 and 3.4.

3.1 The level scheme for ^{213}Ra

The level scheme of ^{213}Ra obtained in the present work is shown in Figure 3.2. The previous work [Rai76, Ras76, Ney94] was used as a reference point for the construction of the level scheme. States up to around 4.5 MeV and J = 35/2 $\hbar$ have been identified, including two new isomeric states. The following sections will explain and justify the assignment of transitions within the level. Note that the initial discussion refers to the spin and parity of states for descriptive purposes, these assignments are not justified until Section 3.4.

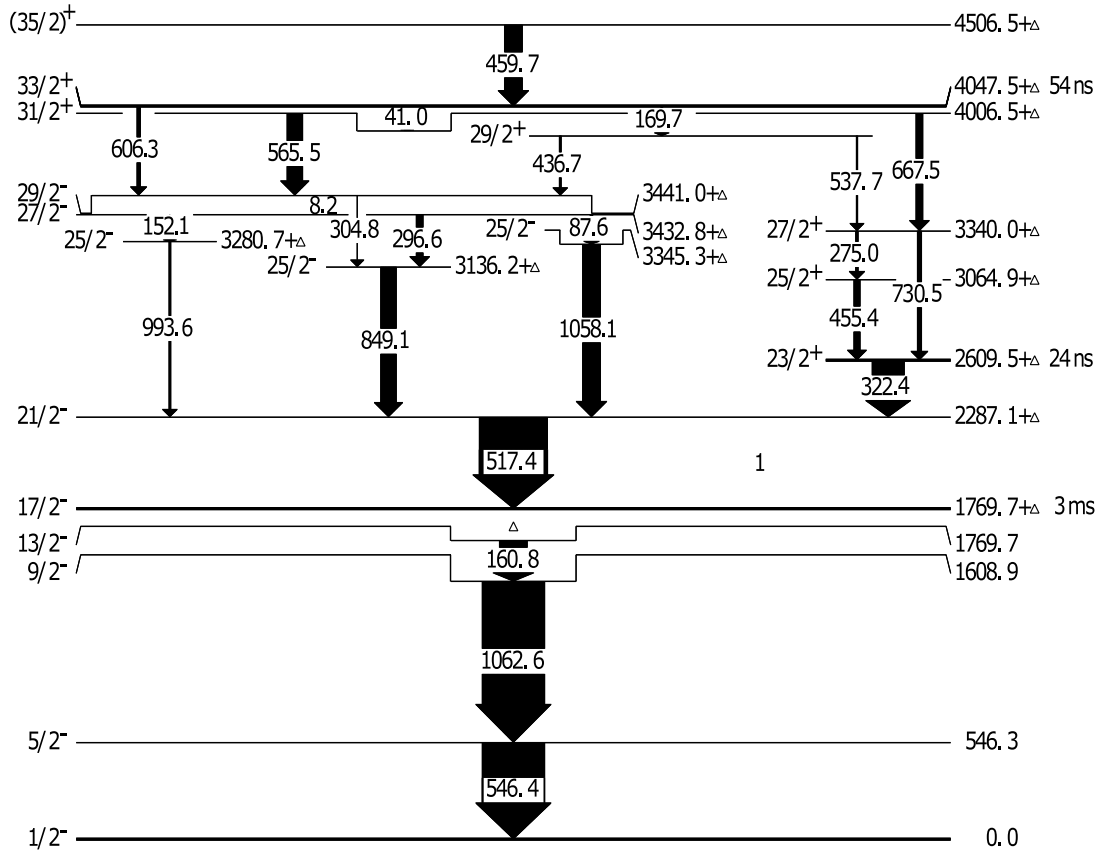

Figure 3.2: Level scheme for ^{213}Ra from the present work. Widths of arrows indicate the relative γ-ray intensities. The parenthesis around the $35/2^+$ state indicates this is a tentative assignment.

3.2 Level scheme above the $17/2^-$ isomer

One of the difficulties in studying nuclei with long-lived isomeric states is the inability to correlate γ-ray decays across the isomer. This is predominantly due to the high number of random coincidences that can take place during the time it takes for the state to decay. The 3 ms isomer in ^{213}Ra falls into this category. The initial focus of the analysis was the 517.44 keV transition. It was easy to assign this as the first transition above the isomer due to its intensity dominating the in-beam spectra. Furthermore, the x-rays coincident with the 517.44 keV, as show in Figure 3.4, match perfectly with the known radium x-rays[1]. A final piece of evidence in this assignment is that when projecting coincidences with the 517.44 γ-ray (Figure 3.4) the resulting spectra contain solely lines that have not yet been assigned to any

[1]The characteristic atomic x-rays of Radium in order of intensity are: 88.47, 85.43, 100.13, 103.00 and 99.43 keV [BEA67]

Table 3.1: The classified transitions between excited states above the $17/2^-$ isomer in ^{213}Ra. The intensities have been fitted using the out-of-beam matrix and are taken relative to the 517.44 keV line. The 8.24, 40.97 and 87.55 keV transitions have not had intensities measured as these transitions are inferred and therefore not present in the out-of-beam matrix. As the 459.66keV transition is prompt-decay it has also not had its intensity measured. The values in parenthesis indicate the uncertainty of the measurement on the smallest scale

Transition energy (keV)	Intensity	Multipolarity	J_i	J_f
8.24 (8)	-	M1	$29/2^-$	$27/2^-$
40.97 (5)	-	M1	$33/2^+$	31/2+
87.55 (4)	-	M1	$27/2^-$	$25/2^-$
152.09 (5)	0.54 (13)	M1	$27/2^-$	$25/2^-$
169.65 (3)	2.89 (17)	E2	$33/2^+$	$29/2^+$
275.02 (4)	2.80 (20)	M1	$27/2^+$	$25/2^+$
296.58 (2)	6.84 (32)	M1	$27/2^-$	$25/2^-$
304.82 (8)	1.73 (16)	E2	$29/2^-$	$25/2^-$
322.38 (1)	43.82(61)	E1	$23/2^+$	$21/2^-$
436.72 (8)	2.54 (20)	E1	$29/2^+$	$29/2^-$
455.36 (4)	6.31 (30)	M1	$25/2^+$	$23/2^+$
459.66 (6)	-	(M1)	$(35/2^+)$	$33/2^+$
517.44 (1)	100	E2	$21/2^-$	$17/2^-$
537.77 (11)	2.14 (21)	M1	$29/2^+$	$27/2^+$
565.50 (2)	44.73 (71)	M1	$31/2^+$	$29/2^-$
606.29 (5)	5.83 (32)	M2	$33/2^+$	$29/2^-$
667.45 (4)	10.90 (40)	E2	$31/2^+$	$27/2^+$
730.51 (5)	6.36 (32)	E2	$27/2^+$	$23/2^+$
849.08 (3)	25.46 (63)	E2	$25/2^-$	$21/2^-$
993.59 (7)	4.02 (27)	E2	$25/2^-$	$21/2^-$
1058.12(2)	30.87 (71)	E2	$25/2^-$	$21/2^-$

nearby nucleus,these transitions are also *all* in coincidence with Ra x-rays. Above the $21/2^-$ state there exist multiple decay paths from the $33/2^+$ state. The following sections will discuss the assignment of transitions and the decay branches above the $21/2^-$ state.

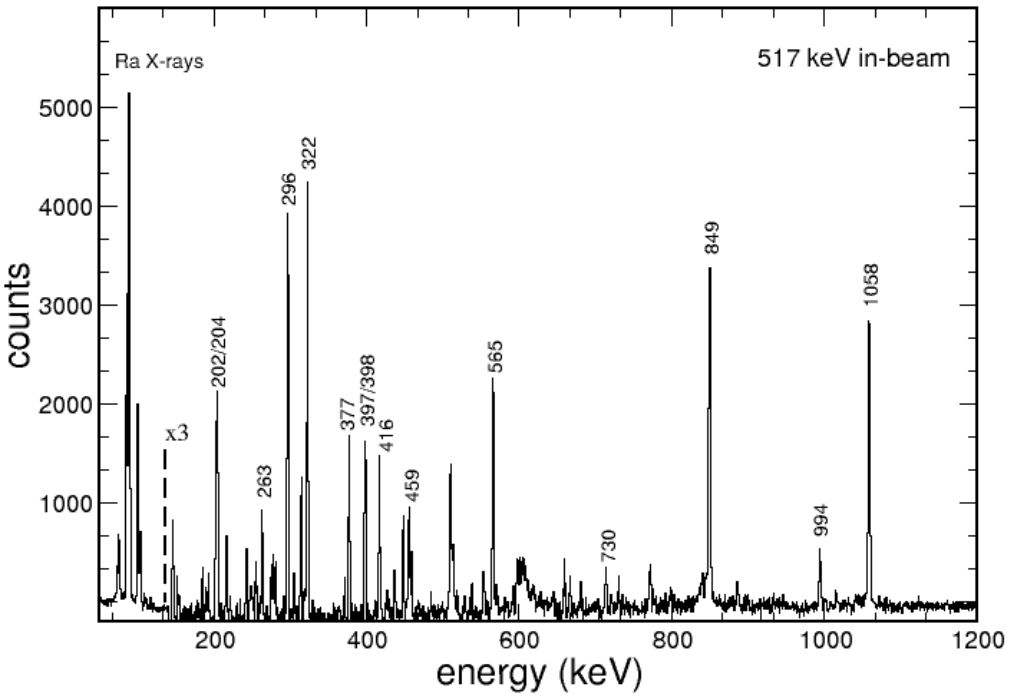

Figure 3.3: Transitions coincident with the 517.44 keV γ-ray in the in-beam matrix.

3.2.1 The 849, 1058 and 994 keV branch

As a nucleus is excited to higher energy, the number of available valence nucleon configurations increases. This gives rise to considerably more complicated nuclear structure as the number of possible states and transitions increases significantly. It is typical for shell model nuclei to exhibit parallel decay cascades which separate and rejoin throughout the level scheme; and potentially, transitions of indistinguishably similar energy. For this reason constructing the level scheme can be a complicated puzzle.

As shown in the 517.44 keV coincidence spectrum (Figure 3.4), the five strongest

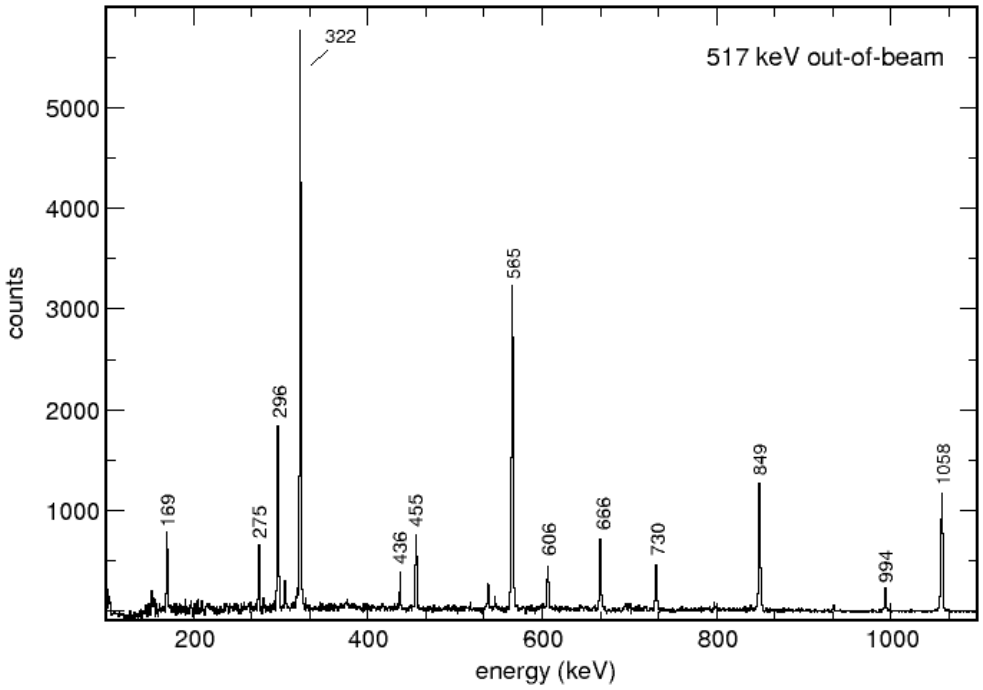

Figure 3.4: Transitions coincident with the 517.44 keV γ-ray in the out-of-beam matrix.

feeding transitions above the $21/2^-$ state are the 296.58, 322.37, 565.50, 849.08 and 1058.12 keV γ-rays. Projecting spectra of decay coincident with each of these lines (Fig 3.5) gives the first evidence of parallel cascade channels within the level scheme. Projecting the coincidences with 1058.12 and 849.08 keV γ-rays shows five peaks common to both spectra at 169.65, 437.72, 517.44, 565.50 and 606.29 keV. This indicates a merging point of the two parallel branches at some state fed by the 169.65, 437.72, 565.5 or 606.29 keV transitions. Since the parallel branches meet at the same state, each branch must sum to the same energy.

The meeting point of the cascades was determined by projecting the coincidence spectra for the 296.58, 849.08 and 1058.12 keV decays. In the 849.08 keV gate there exists a 304.82 keV transition, that is not visible in either the 296.58 or 1058.12 keV coincidence spectra. Consequently the 304.82 keV transition cannot be above or below the 1058.12 keV transition but must be in the same parallel branch as the 849.08 keV line, yet in such a way that the 296.58 keV decay would also not fall in coincidence with it. Looking at the in-beam coincidence spectra for the 304.82 keV

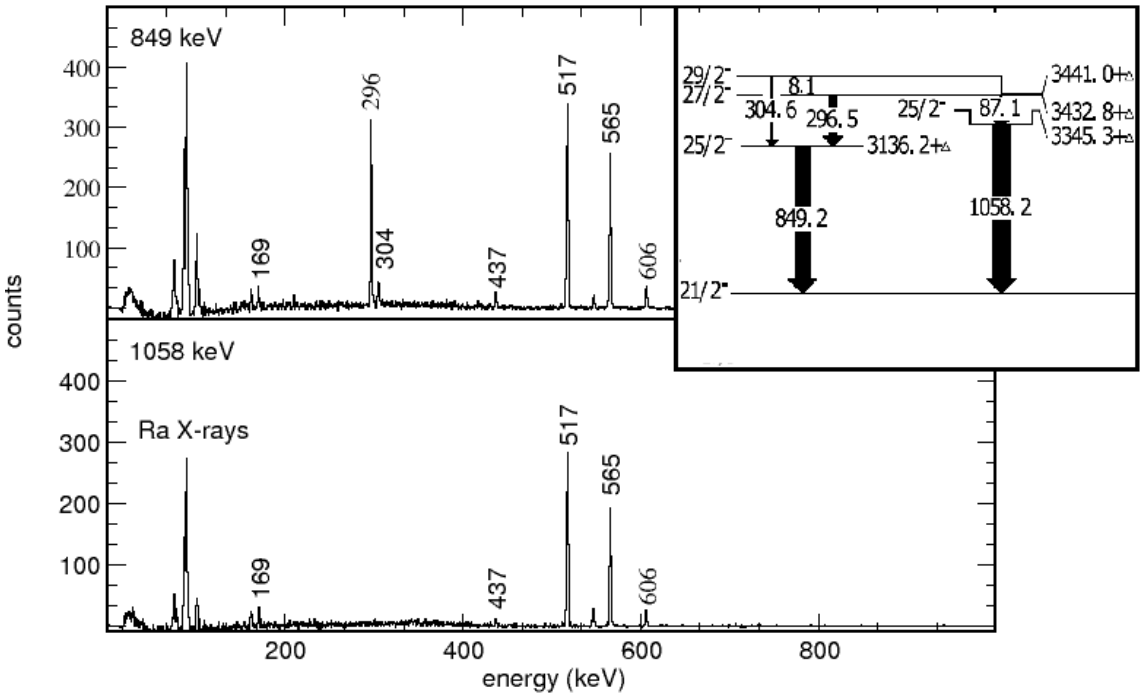

Figure 3.5: Transitions coincident with the 849.08 and 1058.12 keV transitions. The identical spectra above 400 keV indicate that these transitions are part of parallel cascades originating from a higher spin state.

peak (Fig 3.6) we see that it is identical, although weaker in intensity, to that of the 296.58 keV transition. The only logical arrangement is to place the 304.82 keV line parallel to the 296.58 keV line and above the 849.08 keV γ-ray.

As this has resolved the differences in γ-rays coincident with the 849.08 and 1058.12 keV lines, the meeting point of the two branches can be established. The identical 296.58 and 304.82 spectra imply the two sub-branches also meet at the same state. This places an unobserved 8.24 keV gap between the $29/2^-$ and the $27/2^-$ states. The 1058.12 keV decay branch must meet at one of these two states. To determine whether the 1059.12 is fed by a 87.55 keV γ-ray decaying from the $27/2^-$ state or a 95.78 keV transition from the $29/2^-$, coincidence matrices between the LEPS and HPGe detectors were used (x-γ matrices). Fig 3.7 shows gates on the 565.50, 849.08 and 1058.12 keV transitions projecting the coincident LEPS spectra. Because the 87.55 keV γ-ray is not observed in coincidence with the 849.08 it cannot be an x-ray and must in fact be a decay belonging to ^{213}Ra. Furthermore, there is a complete absence of any 95 keV γ-rays in the LEPS spectra. Therefore the 1058.12 keV transition must be fed by an 87.55 keV γ-ray depopulating the $27/2^-$ state.

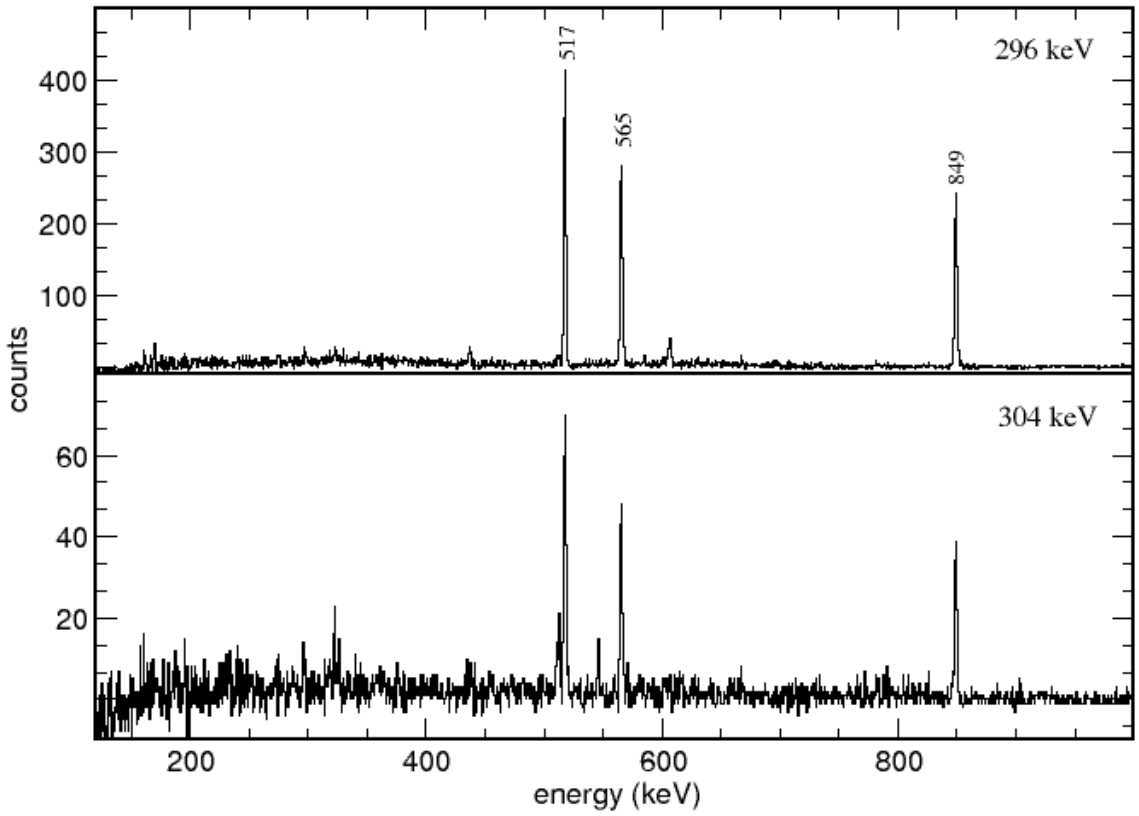

Figure 3.6: γ-rays coincident with the 296.58 and 304.82 keV transitions. The 545 keV transition is a common contaminant in ^{213}Ra coincidence spectra due to the high number of neighboring nuclei with transitions of similar energy. See Section 3.2.6 for further discussion of contaminant transitions

The 993.59 and 152.09 keV γ-rays have been assigned as a parallel decay originating from the $27/2^-$ state using similar reasoning as above. The coincidence spectra (although not shown) are identical to that for the 849.08 and 1058.12 keV γ-rays. Furthermore, the energy sum of each branch depopulating the $27/2^-$ state is 1153.90±0.08, 1153.92±0.09 and 1153.90±0.10. The excellent agreement of these sums and the clear coincidence information provides overwhelming evidence that the unification point of the 849.08, 993.59 and 1058.12 keV parallel cascades can be placed at the 3441.34 keV, $29/2^-$ state.

3.2.2 Identification of a new high-spin isomer

As discussed in Chapter 2, the presence of transitions in the out-of-beam matrix indicates that the γ-rays are fed in the depopulation of an isomeric state. All transitions discussed so far are present in out of beam time cuts, therefore there must

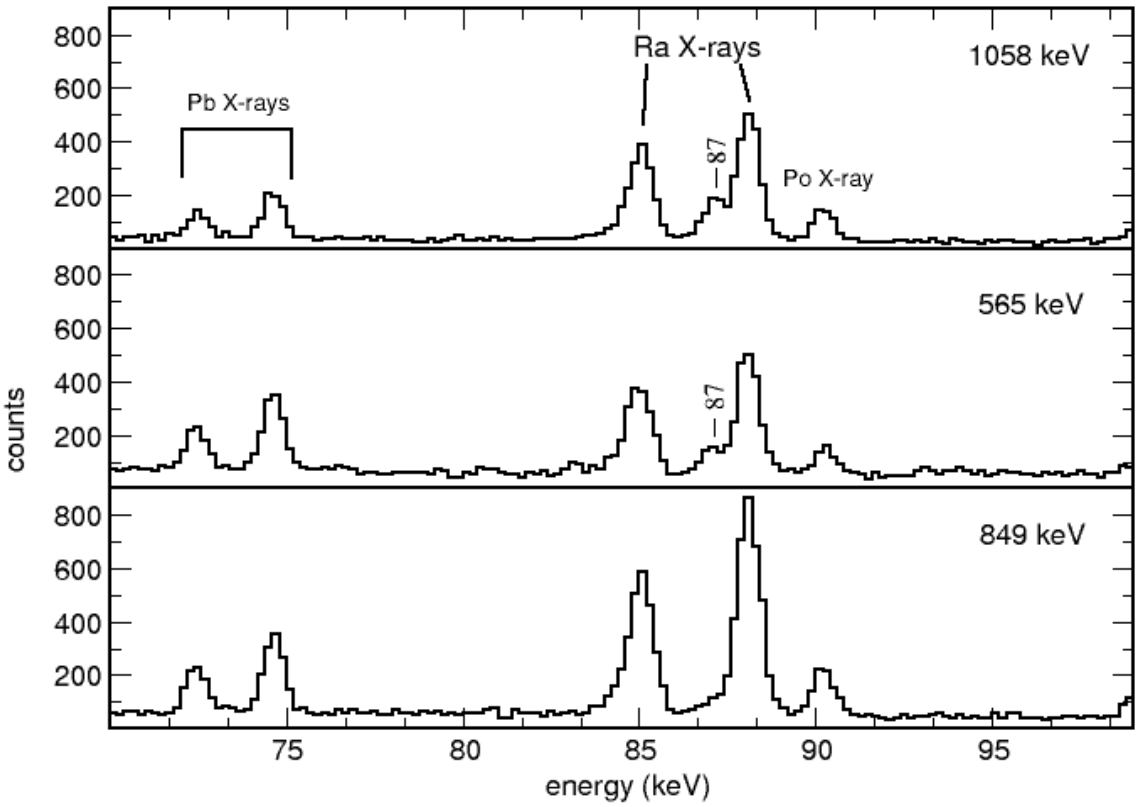

Figure 3.7: LEPS spectra showing the observation of the inferred 87.55 keV γ-ray. Its presence in the 565.50 and 1058.12 keV gates while not being in coincidence with 849.08 keV γ-ray means it cannot be an atomic x-ray.

be a high lying isomer. The 565.50 keV γ-ray is observed in early coincidence with the 296.58, 849.08, 993.59 and 1058.12 keV peaks and has therefore been assigned as the transition feeding the $29/2^-$state. Its appearance in both the early-delayed long and short matrices suggests that it is decay from the isomeric state, however, this conclusion is not altogether certain.

The position of the isomer can be accurately assigned because of the presence of another crossover branch in the level scheme. The 169.65 and 436.72 keV transitions exhibit near identical coincidence spectra to the 606.29 and 565.50 γ-rays. Furthermore the energy sum of 169.65 and 436.72 is 606.37±0.09keV agreeing perfectly with the 606.29 keV γ-ray energy. Therefore these transitions comprise three parallel decay paths from the same state. The presence of these three transitions in out-of-beam coincidence spectra when gating on the 296.58 849.08, 993.59 and 1058.12 keV γ-rays also indicated decay from an isomeric state. Therefore the isomer is not in fact the state from which the 565.50 keV decays but is inferred to be 41 keV above that, i.e. the state from which the 169.65 and 606.29 keV transitions

originate. This, in turn, places an unobserved 41 keV transition between the not yet discussed 33/2+ and 31/2+ states.

3.2.3 The 322 keV branch

The other significant decay branch above the $21/2^-$ state begins with a 322.38 keV transition from the $23/2^+$ isomer. It is immediately obvious that this is a significantly different branch in the level scheme, as the only common coincident transitions between the 322.38 keV path and the 849.08, 993.59, 1058.12keV branches are the 169.65 and 517.44 keV transitions (see Fig. 3.8). Given that the 565.50, 436.72 and 606.29 keV transitions are not shown in coincidence with the 322.38 keV γ-ray, the branch cannot meet at the same $29/2^-$ state. Projecting coincidences with the 322.38 keV transition using the out-of-beam matrices, there are several new strong lines, at 275.02, 455.36, 537.77, 666.45, and 730.51 keV γ-rays. Their placement in the level scheme is discussed below.

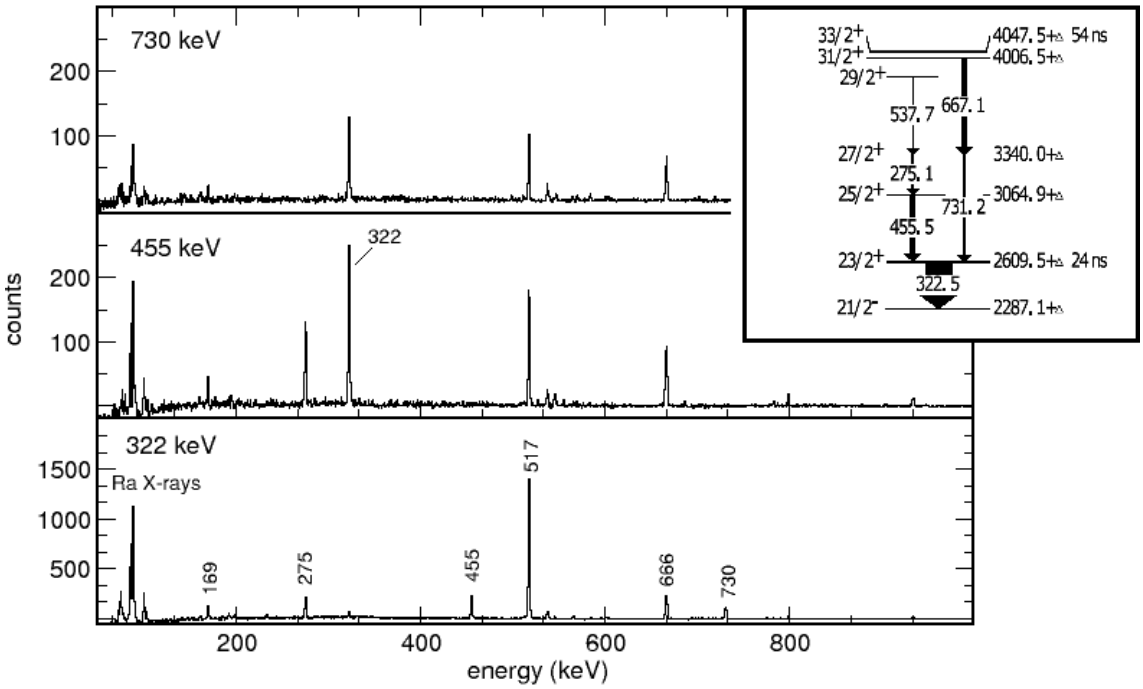

Figure 3.8: Out-of-beam-short cascades in the 322.38 keV branch. The identical coincidence spectra of the 455.36 and 730.51 keV γ-rays place them in parallel above the $23/2^+$ isomer.

The coincidence spectra for the 275.02 and 455.36 keV γ-rays, which sum to 730.38±0.57 keV, reveal that they are coincident with each other but not with the 730.51 keV peak. The matching energy sum makes it easy to assign these γ-rays as two parallel paths depopulating the $27/2^+$ state. This leaves two unassigned transitions in the 322.38 keV branch, the 666.45 and 537.77 keV γ-rays. These transitions are also assigned in parallel on the same basis. They do not, however, meet at the same state.

The 537.77 keV transition is coincident with the 169.65 γ-ray decaying from the $33/2^+$ isomer, while the 666.45 keV γ-ray is not. This means the 322.38 keV branch has to intersect with the crossover branch at the $29/2^+$ state. Summing the energies of the decay through the 322.38 keV branch with the 537.77 keV γ-ray gives 3878.06±0.12 keV, the energy of the $29/2^+$ state. This firmly assigns the 537.77 as the transition depopulating the $29/2^+$ state and feeding into the 322.38 keV branch. Using similar energy arguments the 666.45 keV γ-ray is assigned as decaying directly from the $31/2^+$ state. The energy sum of the left hand branch in the level scheme is 4006.84±0.04 keV, the energy sum of the 666.45 and the rest of the 322.38 keV branch is 4006.78±0.07 keV. This excellent agreement confirms the assignment of the 666.45 keV transition as decaying from the $31/2^+$ state.

3.2.4 States above the $33/2^+$ isomer

Above there $33/2^+$ isomer there has been one transition assigned to the level scheme. The assignment of the 459.66 keV γ-ray is based on its early coincidence relationship with the 565.5 and 667.45 keV transitions. The positive parity assignment of the $J = 35/2\hbar$ state is at this stage tentative as angular distributions for the 459.66 keV transition have only indicated that it is a dipole transition (i.e. it could be E1 or M1). Further assignment of prompt decay above the $33/2^+$ has not yet been possible due to a number of issues discussed in the next section.

3.2.5 Concerning tentative and unassigned transitions

There are many transitions in the in-beam coincidence spectra for the 517.44 keV (Figure 3.3) transition that are not yet placed in the level scheme (Figure 3.2).

These γ-rays, while belonging to ^{213}Ra, can not be confidently assigned for various reasons. Foremost, the transitions do not originate from the isomeric $33/2^+$ state. They are therefore not present in out-of-beam spectra and consequently their coincidence spectra are less clean with considerable background. A table of unassigned γ-rays is presented below in Table 3.2. Further complications arise due to the existence of two close lying doublet transitions at 202/204 keV and 397/398 keV. The difficulty in resolving these transitions has, to date, made it impossible to determine the ordering and γ-ray coincidences of each pair. To make matters worse, early-delayed coincidences with the 202/204 keV pair are dominated by contaminant γ-rays because of the 203.1 keV transition from the 8^+ to 6^+ isomeric states in ^{210}Rn [Pol05], which were relatively strongly populated.

Table 3.2: The tentatively assigned transitions in ^{213}Ra. Limited numerical precision has been used in the numbers reported due to their tentative nature. Superscript symbols denote transitions in the same cascade.

Transition energy (keV)	Initial state energy (keV)	Final state energy (keV)	Notes on assignment
202°	3643	3441	Parallel to 416 and 565
204$^{\circ\bullet}$	3847	3643	Parallel to 565
208	3345	3136	Crossover between 849 and 1059 branch
216	-	-	Parallel to 565
280	4327	4047	Above $33/2^+$ isomer
263°	-	-	In cascade with 202/204 doublet
314	-	-	-
376*	3402	3026	low intensity decay from $29/2^-$ state
377^{X}	-	-	Above $33/2^+$ isomer
397^{X}	-	-	Above $33/2^+$ isomer
398^{X}	-	-	Above $33/2^+$ isomer
416$^{\bullet}$	3857	3441	Parallel to 202 and 565
447	-	-	Above $33/2^+$ isomer
509	-	-	-
513	-	-	-
584	-	-	coincident with Ra x-rays and strong 296 keV γ-ray
675*	2347	1672	-
679*	3026	2347	-
798	3407	2609	Low intensity decay feeding $23/2^+$ state
934	3543	2609	Low intensity decay feeding $23/2^+$ state
1126*	1672	546	decay cascade going around $17/2^-$ isomer

Their is some limited evidence for the way in which the transitions have been assigned in this table, with coincidence information presented that has been carefully extracted from the data. There are, however, inconsistencies and potentially implausible relationships where more information is required to firmly determine the structure of the level scheme. Many coincidences are unique to particular transitions, possibly implying the γ-ray may be contaminated by transitions from other nuclei. The low intensity of these lines means the atomic x-rays are often not visible inhibiting correct identification of the parent nucleus.

Due to time constraints, further investigation of the tentatively assigned gamma-rays could not be completed. The transitions documented have been, for the most part, confirmed to belong to ^{213}Ra. A complete investigation of the remaining transitions is left as work for the future.

3.2.6 Contaminant radiation from reaction products

In heavy-ion fusion experiments the reaction will form a range of products in addition to the desired nucleus. The hot excited nucleus will evaporate particles to cool down. Evaporated particles will typically be neutrons, although the emission of charged particles such as protons, or even α-particles, is also possible. Another competing process is the fission of the compound nucleus. The desired reaction in this work was ^{204}Pb(^{13}C,4n)^{213}Ra. Table 3.3 shows observed contaminant products as well as the reactions that produced them. Figure 3.9 graphically illustrates the various reaction channels.

Table 3.3: Identified contaminant transitions from neighboring nuclei. Observed γ-ray energies taken from Refs. [Pol05, Dav93, Pol00, Stu92]. This table does not include all contaminant transitions found, only those which were most prevalent.

Nucleus	Transition energy (keV)	Reaction
^{210}Rn		^{204}Pb(^{13}C,α3n)^{210}Rn
	119.7	
	203.1	
	325.4	
	545.7	
	564.3	
	643.9	
	712.3	
	817.8	
	901.2	
^{211}Rn		^{204}Pb(^{13}C,α2n)^{211}Rn
	119.6	
	511.5	
	536.3	
	539.9	
	569.9	
	584.2	
	601.0	
	569.9	
	918.3	
	994.7	
^{209}Po		^{204}Pb(^{13}C,4nα2β)^{209}Po
	195.3	
	206.5	
	239.4	
	325.6	
	545.1	
	782.3	
	790.6	
	1104.1	
^{214}Ra		^{204}Pb(^{13}C,3n)^{214}Ra
	146.5	
	208.7	
	321.9	
	775.1	
	666.3	
	668.4	

Contaminant radiation can produce apparently false coincidences due to energeti-

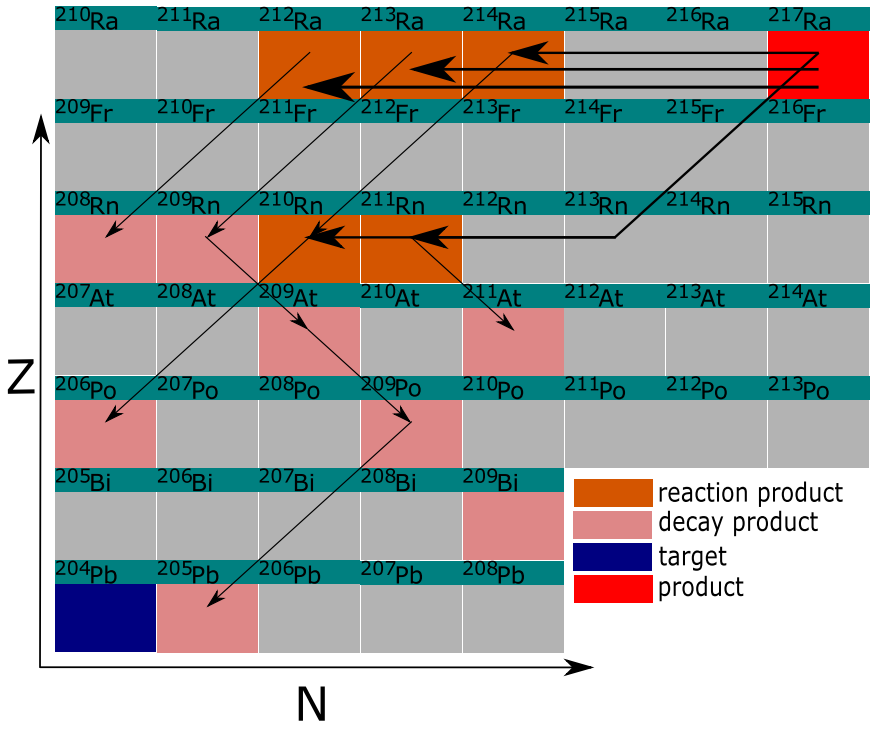

Figure 3.9: Identified contaminant reaction products from the ^{13}C + ^{204}Pb heavy-ion reaction. The ^{204}Pb target was enriched to greater than 99% placing an upper-bound on the mass of reaction products at ^{217}Ra. The solid arrows indicate the paths to the direct reaction products, the other arrows indicate the path of decay from each nucleus.

cally similar transitions. In order to correctly interpret spectra it is important to address the contaminant transitions. Two prominent examples are ^{210}Rn and ^{214}Ra. False coincidences are generated with ^{210}Rn because of three energetically similar transitions to ^{213}Ra, these are the 564.3, 545.7 and 203.1 keV transitions. Their prominence is due to two long isomers in ^{210}Rn; the τ = 1530 ns state from which the 564.3 decays and the τ = 929 ns isomer from which the 203.1 keV γ-ray originates. Further isomeric contaminants are found in ^{209}Po with its 545 keV γ-ray and in ^{214}Ra with a 321.9 keV transition and a 668.4 keV transition. The contaminant coincidences do not just mean that the energetically similar γ-rays will appear in the spectra, but all transitions coincident with the contaminant radiation as well. The 565.50 keV coincidence spectrum in particular was dominated by both long lived and prompt coincidences with ^{210}Rn lines due to its 564.3 keV transition, complicating the analysis of less prominent spectral features. Identification of contaminant nuclei and radiation is often sufficient to disregard their appearance in ^{213}Ra spectra, how-

ever, it is sometimes necessary to subtract contaminant spectra from the spectra of interest to produce clean, contaminant free results at the expense of statistics and increasing background fluctuations.

3.3 Lifetime measurements of isomeric states

This section will discuss the measurements for the two isomers observed in ^{213}Ra. Lifetimes were determined using the methods outlined in Chapter 2. Figures 3.10 and 3.11 show the two lifetimes determined.

3.3.1 The $23/2^+$ isomer

The prominence of the 322.28 keV transition gave rise to clean gated spectra allowing easy determination of the $23/2^+$ state's lifetime. The γ-γ-ΔT spectrum with gates on the 517.44 and 455.36 keV γ-rays was used, giving a lifetime of 24.6±0.5 ns as shown in Figure 3.10.

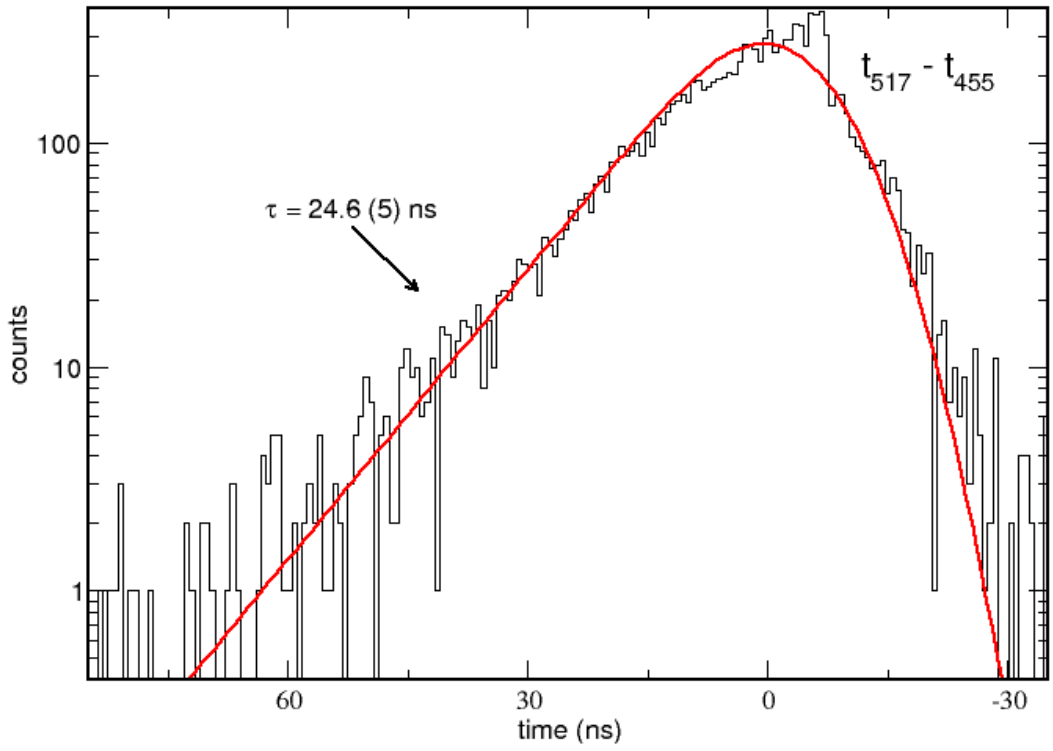

Figure 3.10: The lifetime measurement of the $23/2^+$ isomer from the time difference spectrum between the 517.44 and 455.36 keV transitions.

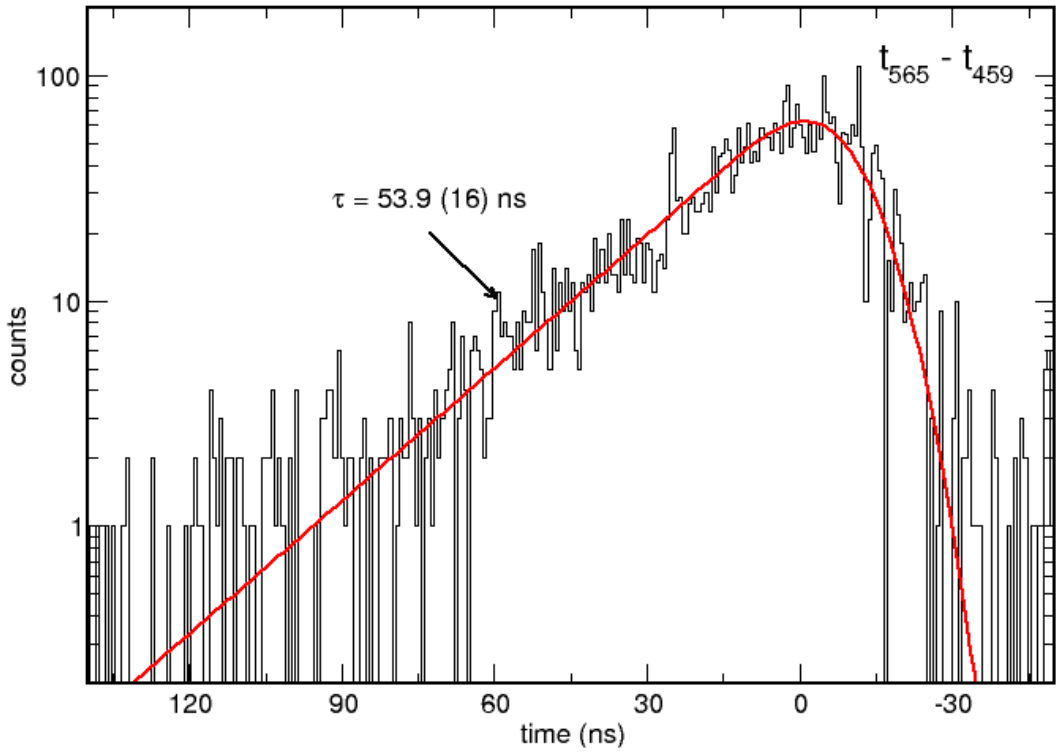

Figure 3.11: The lifetime measurement of the $33/2^+$ isomer made using the time difference spectra for the 565.5 and 459 keV transitions.

3.3.2 The $33/2^+$ isomer

The lifetime measurement of the $33/2^+$ isomer was again made using the γ-γ-ΔT method. The time difference between the 565.50 and 459 keV γ-rays gives the lifetime of the state as 53.9$\pm$1.6 ns. This value is consistent with expectations based on the out-of-beam coincidence matrices that suggest this high-lying isomer would exhibit a longer lifetime than the $23/2^+$ state.

In the case of either isomer, taking the lifetime with respect to the pulsed beam yields inconsistent results. For both states the measured lifetime is longer than when made using the γ-γ-time difference method. Beyond this, using the beam pulsing method with respect to the 322.28 keV transition can only result in a lifetime curve exhibiting the decay components of both the $23/2^+$ and $33/2^+$ isomers. This behavior is shown in Fig 3.12. In the short time frame avaliable, this ambiguity has not yet been resolved. The γ-γ-ΔT method gives confident measurement of the state lifetimes as it isolates the induvidual states. For this reason lifetimes deduced using the γ-γ-ΔT method have been adoped in the level scheme.

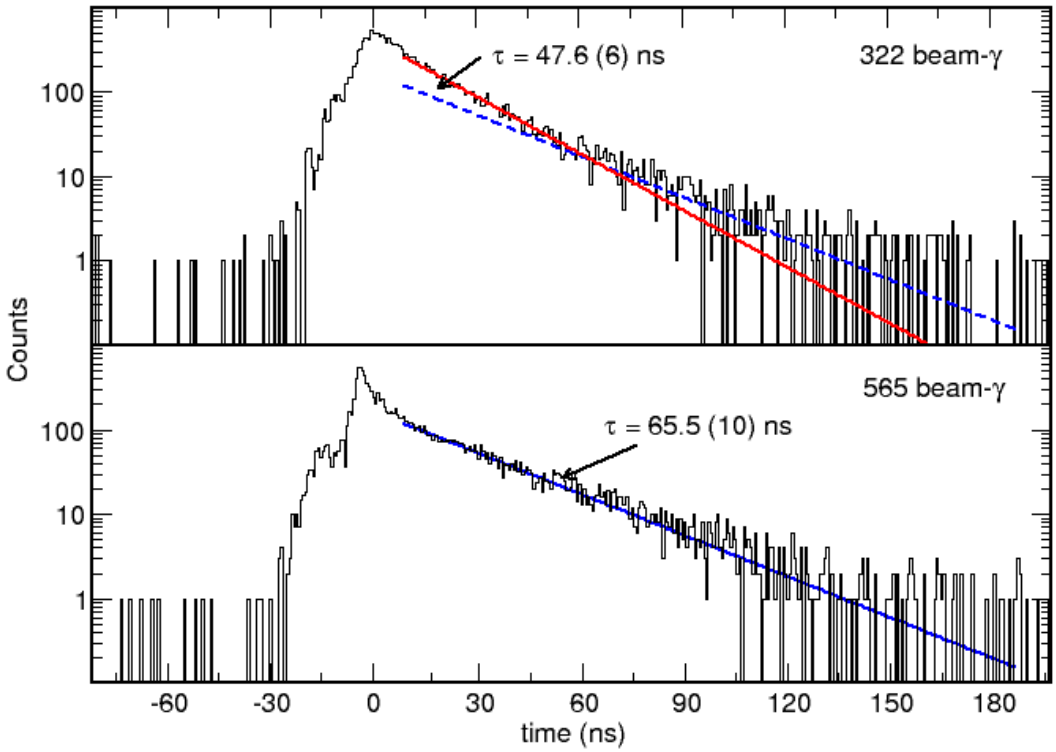

Figure 3.12: The ambiguous beam-γ lifetime measurements for the $33/2^+$ and $23/2^+$ isomers. The dotted blue line in the 322 beam-γ plot indicates the unexplained influence of the $33/2^+$ isomer. Due to side feeding from short-lived states there is a prompt peak component centered near $\tau = 0$ in both spectra.

3.3.3 Transition strengths of isomeric decay

Shown below is a table of measured transition strengths for the γ-rays decaying from the isomeric $23/2^+$ and $33/2^+$ states. These will be discussed with reference to configuration assignments in Chapter 4.

Table 3.4: A table of transition strengths (in W.u) for the isomeric states. A smaller transition strength relative to γ-rays from the same state implies a stronger transition.

State	Transition (keV)	Branching ratio	Multipolarity	Strength (W.u)
$33/2^+$, τ = 53.9(16)				
	40.97	84	M1	$170(8)\times10^{-6}$
	169.65	7	E2	$50(9.4)\times10^{-3}$
	606.29	9	M2	$19(2.4)\times10^{-3}$
$23/2^+$, τ = 24.6(5)				
	322.38	100	E1	$29(6)\times10^{-8}$

3.4 Spin and parity assignments

This section will describe the spin and parity assignments shown in Table 3.1, using the techniques outlined in Chapter 2. It should be noted that only angular distributions for decay present in the in-beam matrices can be measured. This is because the long time cut used in the out-of-beam matrices samples over a region where the anisotropy might be attenuated. Consequently the multipolarity of the 169, 437 and 606 keV transitions can not be determined directly from the data and are instead inferred from the assignments of other decays in the level scheme. Table 3.5 shows the multipolarities, values of A2/A0 and internal conversion coefficients ofor the transitions adopted in the level scheme. Angular distributions for the 517.44, 322.38, 849.08 and 537.77 keV transitions are shown in Fig 3.13. Figure 3.14 shows a comparison of calculated internal conversion coefficients with theoretical predictions made using the BrIcc software package from Ref. [Kib08].

Table 3.5: Measured angular distributions and inferred internal conversion coefficients for transitions in ^{213}Ra

Transition energy (keV)	$\frac{A_2}{A_0}$	Multipolarity	α_T
8.24	-	M1	-
40.97	-	M1	-
87.55	-	M1	-
152.09	-	M1	3.677±0.56
169.65	-	E2	0.671±0.18
275.02	-0.41±0.02	M1	0.644±0.07
296.58	-0.73±0.04	M1	0.962±0.09
322.38	-0.31±0.05	E1	0.11±0.05
436.72	-	E1	-
455.36	-1.056±0.06	M1	-
517.44	0.264±0.01	E2	-
537.77	-0.459 ± 0.07	M1	-
565.50	-0.459±0.06	M1	-
606.29	-	M2	-
667.45	0.38±0.13	E2	-
730.51	0.38±0.17	E2	-
849.08	0.38±0.04	E2	-
993.59	0.33±0.14	E2	-
1058.12	0.3±0.05	E2	-

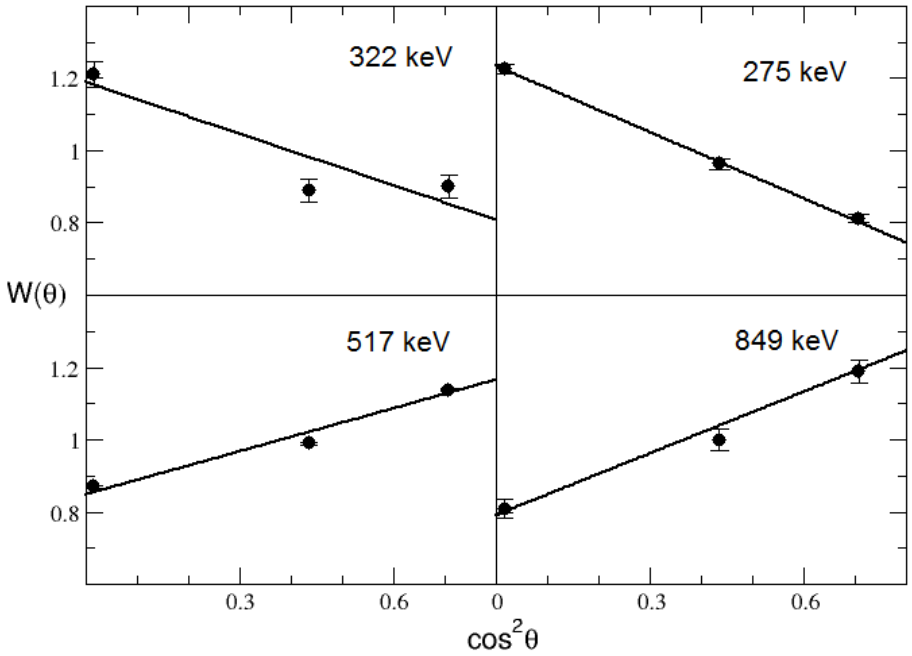

Figure 3.13: The angular distributions for the 322(a), 275(b), 517(c), 849(d) keV transitions plotted as a function of $\cos^2\theta$.

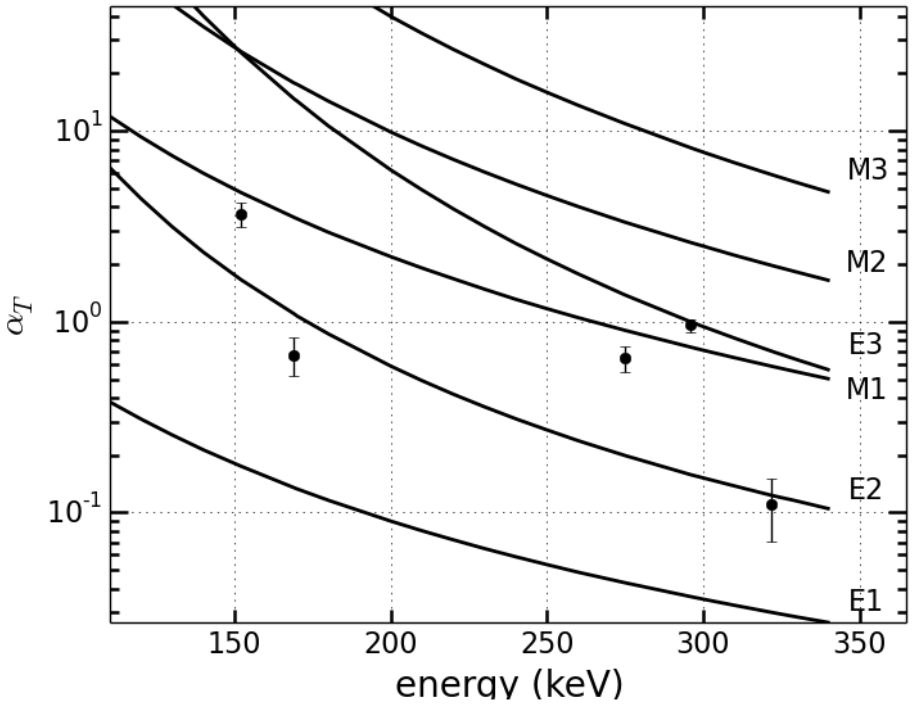

Figure 3.14: Comparison of experimental internal conversion coefficients against theoretical predictions using BrIcc from Ref. [Kib08].

3.4.1 Spin assignments in the negative parity branch

The structure of the level scheme splits into two cascades below the $33/2^+$ isomer, one where all states exhibit positive parity and one with negative parity states. It is natural to discuss spin assignments within each branch separately as each branch corresponds to a significantly different configuration of valence nucleons.

Angular distributions measured for the 517.44, 849.08, 1058.12 and 993.59 keV transitions strongly support quadrupole assignments. Given that none of these states exhibits a measurable lifetime it must be the case that they are all E2 transitions since, from Weisskopf estimates (Section 1.5), M2 transitions will typically exhibit longer lifetimes. The 517.44 γ-ray having E2 multipolarity firmly assigns the 2287.44 keV state to have spin and parity $21/2^-$. It follows that the states from which the 849.08, 993.59 and 1058.12 keV gamma-rays decay must have spin and parity $25/2^-$ as these are all E2 transitions.

Internal conversion coefficients indicate that the 152.09 and 296.58 keV transitions feeding two of the $25/2^-$ states are both M1. This discovery allows the confident assignment of $27/2^-$ to the 3434 keV state. The unobserved 8.24 keV γ-ray has been given M1 multipolarity on the basis that such a low energy E1 or E2 transition would typically exhibit a lifetime (i.e imply an isomeric state). As this state is not an isomer, this suggests it has a spin and parity $29/2^-$. The 565.50 keV γ-ray is assigned as an E1 based on the dipole nature of its angular distribution and inferences from the positive parity branch, which will be discussed in the next section.

3.4.2 Spin assignments in the positive parity branch

The change to positive parity corresponds to the excitation of a proton from the $h_{9/2}$ orbit to the $i_{13/2}$ orbit. Thus all configurations in this branch correspond to the coupling of the $i_{13/2}$ proton. The first transition from a positive parity state is the 322.38 keV γ-ray. This transition has α_T implying either an E2 transition or, at the 2σ limit an E1 transition. However, the value of A2/A0 suggests dipole character which implies E1 multipolarity. The observed lifetime for the state is also more consistent with an E1.

Angular distributions measured for the 275.02 and 455.36 keV γ-rays strongly indi-

cate dipole transitions. The calculated internal conversion coefficient for the 275 keV decay indicates that it is magnetic in nature and agrees with the dipole assignment. This assigns the spins and parities of the 3065.18 and 3340.20 keV states as $25/2^+$ and $27/2^+$, respectively. The 730 keV transition above the $23/2^+$ state exhibits a quadrupole angular distribution. This is consistent with the implied $23/2^+$ to $27/2^+$ spin change and hence, this transition is confirmed as an E2.

No angular distribution can be measured for the 169.65 keV transition depopulating the isomeric level due to loss of alignment through hyperfine interactions, however, an internal conversion coefficient can be calculated by gating on the 322.38 keV line and balancing the intensity of the 169.65 and 537.77 keV γ-rays[2]. As a further complication, no internal conversion coefficient could be determined for the 537.77 keV γ-ray due to its high energy. This meant that, in order to balance the total intensity feeding and exiting the $29/2^+$ state, the internal conversion coefficients had to be calculated twice, once assuming the 537.77 keV γ-ray was an E1 and once assuming it was a M1 transition. Treating the 537.77 keV γ-ray as an M1 gave the most plausible result[3] for the internal conversion coefficient of the 169.65, corresponding to it being an E2 transition. Higher multipolarity options for the 537.77 keV γ-ray were not considered as the angular distribution of the transition indicated that it was a dipole.

Multipolarities of the remaining 40.97, 436.72, 565.5 and 666.45 keV γ-rays can now be inferred using the spin and parity assignments already discussed. The 40.97 keV M1 assignment makes sense because it carries most of the intensity through this channel. Any higher multipolarity would not be competitive with the competing 606.29 keV M2 and the 169.65 keV E2 decays. Furthermore, were it an E1 the lifetime observed would have been several orders of magnitude longer as E1 transitions in the valence space are heavily hindered. This assigns the spin and parity of the 4006.48 keV state to be $31/2^+$. From this assignment it follows that the 565.5 and 666.45 keV γ-rays decaying from it have multipolarity M1 and E2 respectively. Given that the $29/2^+$ state decays to a $29/2^-$ state via the 436.72 keV γ-ray this transition must be an E1 as there is a parity flip with no spin change.

[2]the 436.72 keV transition was due to its weak intensity and it not being present in the in-beam matrices used to determine the angular intensity of emitted radiation

[3]Treating the 537.77 keV γ-ray as an M1 results in a deviation of 17% with theoretical values compared with a deviation of 40% when considering it an E1.

Chapter 4
The structure of ^{213}Ra

This chapter discusses the states predicted to occur in ^{213}Ra from the semi-empirical shell model. These calculations will attempt to reproduce excited states in the level scheme in terms of different configurations and couplings of the valence nucleons. Justification for spin and parity assignments in the experimental level scheme, as well as the agreement of theory and experiment, will be examined herein. The computer code used for the semi-empirical shell model calculations was written by A.E Stuchbery [Ref].

4.1 The calculated level scheme

The states observed in ^{213}Ra can often be related to those in ^{214}Ra through the coupling of an additional $p_{1/2}$ (or $f_{5/2}$) neutron hole. For this reason, we expect the states and configurations in ^{213}Ra to be similar to those of the closed neutron shell case, ^{214}Ra. Figure 4.1 shows the theoretically predicted states in ^{213}Ra grouped according to the underlying configurations of valence nucleons. These calculations are juxtaposed with states from the experimentally determined level scheme. For low-spin states the predicted energy will often differ significantly from the experimentally measured energy. This is because the present calculation only considers the contribution and interaction of one configuration of valence nucleons. In practice and, as is shown in this chapter, there are many possible configurations that can give rise to excited states. The interaction and hence mixing of different configurations is important in some cases and its neglect causes discrepancies with experiment.

The ground state is particularly affected as there are many ways a configuration can minimally couple to zero. At intermediate spin the agreement between experimental and theoretical energies will be best as many of the configurations will be unique. However, regardless of spin, significant levels of configuration mixing will occur whenever there are many possible ways of exciting nucleons to produce states of a given. The higher-lying configurations tested in this work correspond to permutations of the excitation of a single proton out of the $h_{9/2}$ orbital and into the $f_{7/2}$ or $i_{13/2}$ orbitals, as well as the excitation of an $f_{5/2}$ neutron into the $p_{1/2}$ shell. The latter excitation is equivalent to the excitation of a $p_{1/2}$ neutron into a $f_{5/2}$ hole (see Figure 1.5).

Shown below is a table summarising the configuration assignments and the root-mean-squared (RMS) agreement of theory and experiment.

Table 4.1: Configuration assignments based on energetic agreement between the predicted and experimental structure of ^{213}Ra. The RMS deviation is for states above $J^{\pi} = 17/2^{-}$ as low lying configurations are dominated by the effects of configuration mixing. An alternative $33/2^{+}$ configuration, indicated by the '*', has been included as this state appears to be heavily mixed thus lowering the experimentally observed energy.

State (keV)	Measured Energy (keV)	Predicted Energy (keV)	Agreement (keV)	Configuration
$1/2^{-}$	0	384	384	$(\pi h_{9/2})^{6} \otimes (\nu p_{1/2})^{-1}$
$5/2^{-}$	546	1105	559	$(\pi h_{9/2})^{6} \otimes (\nu f_{5/2})^{-1}$
$9/2^{-}$	1609	1741	132	$(\pi h_{9/2})^{6} \otimes (\nu p_{1/2})^{-1}$
$13/2^{-}$	1770	1862	92	$(\pi h_{9/2})^{6} \otimes (\nu p_{1/2})^{-1}$
$17/2^{-}$	1770 + Δ	1881	110	$(\pi h_{9/2})^{6} \otimes (\nu p_{1/2})^{-1}$
$21/2^{-}$	2287 + Δ	2548	259	$(\pi h_{9/2})^{6} \otimes (\nu f_{5/2})^{-1}$
$23/2^{+}$	2610 + Δ	2492	-119	$(\pi h_{9/2})^{5} \otimes (\pi i_{13/2}) \otimes (\nu p_{1/2})^{-1}$
$25/2^{-}$	3136 + Δ	3007	-131	$(\pi h_{9/2})^{6} \otimes (\nu p_{1/2})^{-1}$
$25/2^{-}$	3281 + Δ	3259	79	$(\pi h_{9/2})^{5} \otimes (\pi f_{7/2}) \otimes (\nu p_{1/2})^{-1}$
$25/2^{-}$	3345 + Δ	3426	-23	$(\pi h_{9/2})^{6} \otimes (\nu f_{5/2})^{-1}$
$25/2^{+}$	3064 + Δ	3107	41	$(\pi h_{9/2})^{5} \otimes (\pi i_{13/2}) \otimes (\nu f_{5/2})^{-1}$
$27/2^{-}$	3433 + Δ	3379	-55	$(\pi h_{9/2})^{5} \otimes (\pi f_{7/2}) \otimes (\nu p_{1/2})^{-1}$
$27/2^{+}$	3340 + Δ	3464	123	$(\pi h_{9/2})^{5} \otimes (\pi f_{7/2}) \otimes (\nu p_{1/2})^{-1}$
$29/2^{-}$	3441 + Δ	3389	-53	$(\pi h_{9/2})^{5} \otimes (\pi f_{7/2}) \otimes (\nu f_{5/2})^{-1}$
$29/2^{+}$	3888 + Δ	3339	-41	$(\pi h_{9/2})^{5} \otimes (\pi i_{13/2}) \otimes (\nu p_{1/2})^{-1}$
$31/2^{+}$	4006 + Δ	3886	-122	$(\pi h_{9/2})^{5} \otimes (\pi i_{13/2}) \otimes (\nu p_{1/2})^{-1}$
$33/2^{+*}$	4047 + Δ	4379	330	$(\pi h_{9/2})^{5} \otimes (\pi i_{13/2}) \otimes (\nu p_{1/2})^{-1}$
$33/2^{+*}$	4047 + Δ	4330	281	$(\pi h_{9/2})^{5} \otimes (\pi i_{13/2}) \otimes (\nu f_{5/2})^{-1}$
$35/2^{+*}$	4506 + Δ	4592	86	$(\pi h_{9/2})^{5} \otimes (\pi i_{13/2}) \otimes (\nu p_{1/2})^{-1}$
$35/2^{+*}$	4506 + Δ	4482	24	$(\pi h_{9/2})^{5} \otimes (\pi i_{13/2}) \otimes (\nu f_{5/2})^{-1}$
RMS deviation (keV)	-	-	139	-

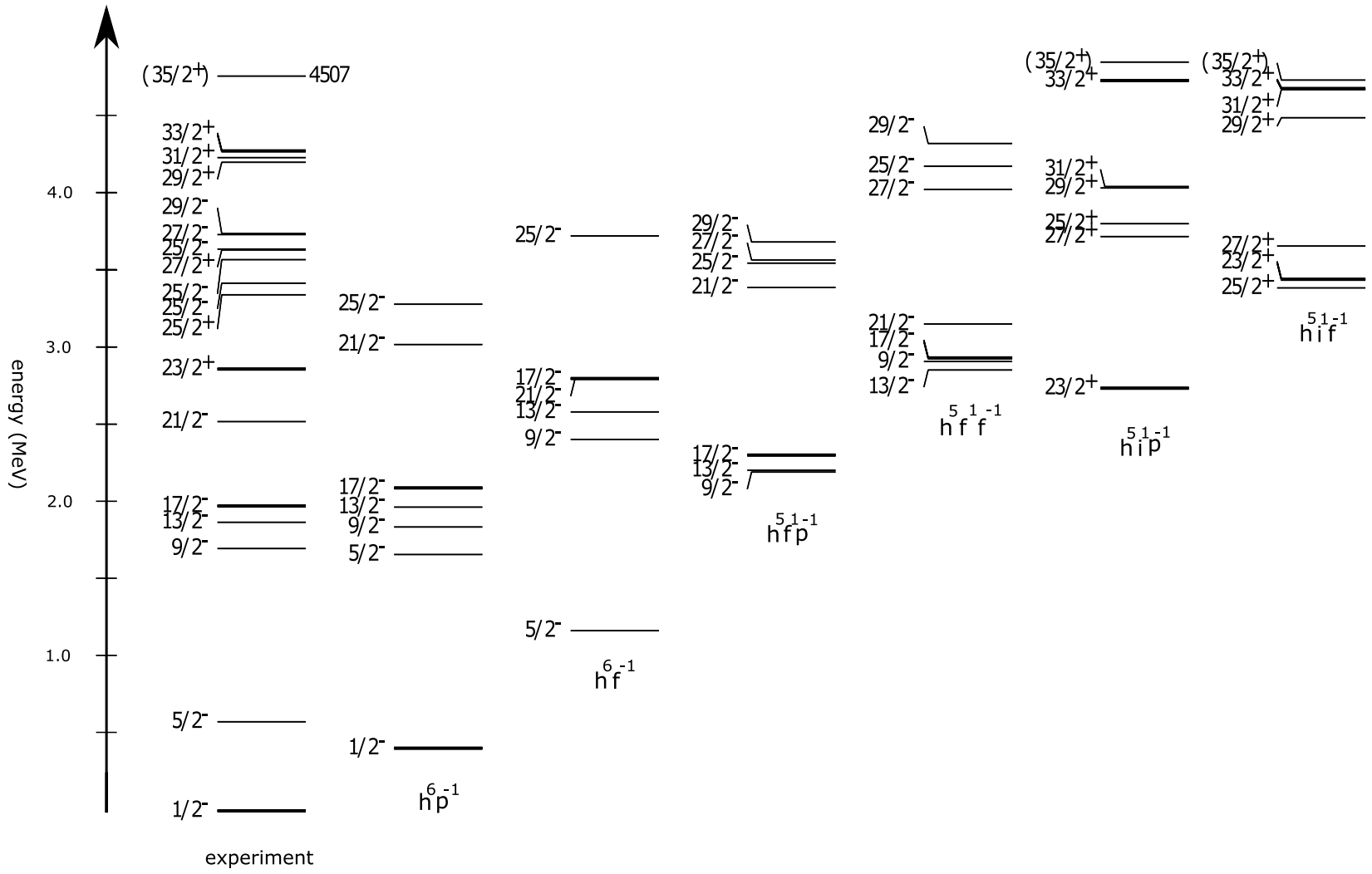

Figure 4.1: The experimentally determined level scheme shown with predictions for various nucleon configurations ordered from left to right with increasing excitation energy. The configurations have been short handed to: h^n for $h_{9/2}$, f^1 for $f_{7/2}$, p^{-1} for $p_{1/2}$, f^{-1} for $f_{5/2}$ and i^1 for an $i_{13/2}$ excitation.

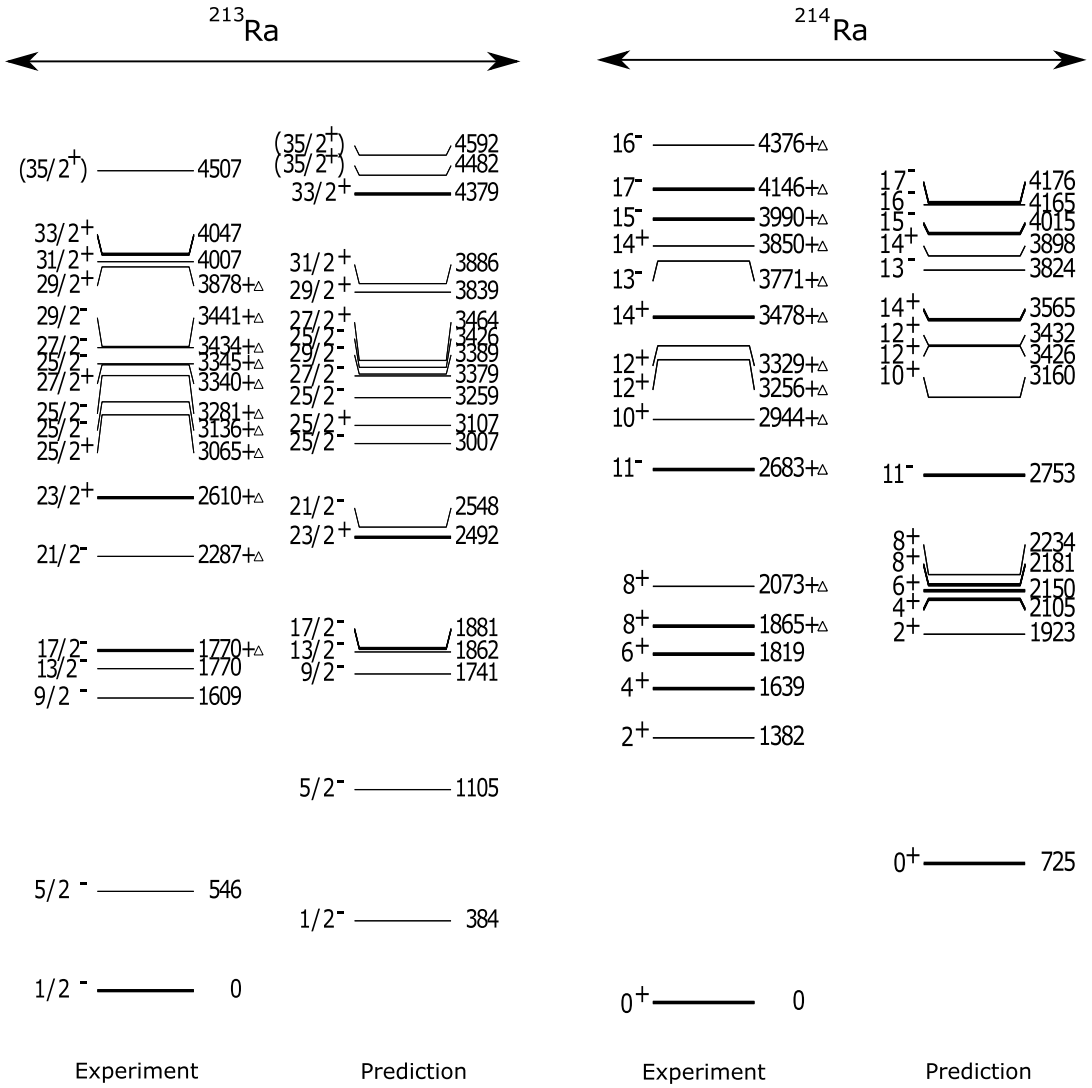

Figure 4.2: Comparison of ^{213,214}Ra experimentally measured levels beneath the 17^- / $35/2^+$ states and the semi-empirical shell model predictions for each nucleus, the latter selecting particular assigned configurations from the complete ^{213}Ra calculation in Figure 4.1 see Ref. [Stu92] for complete ^{214}Ra calculation

4.2 Configuration assignments

The ground state configuration of ^{213}Ra is nominally[1] given by $(\pi h_{9/2})^6_0 \otimes (\nu p_{1/2})^{-1}_{1/2}$. This configuration gives rise to the low-excitation negative parity states observed, and the predicted excited-state energies match closely with the observed values for the $9/2^-$,$13/2^-$ and $17/2^-$ states (as shown in Figure 4.2). D. Raich et al [Rai76] suggested the $5/2^-$ state corresponded to the $p_{1/2}\nu^{-1}$ into a $f_{5/2}\nu^{-1}$ excitation. The calculation confirms this assignment as the energy of the observed $5/2^-$ state is best matched at 1105 keV by the $(\pi h_{9/2})^6_0 \otimes (\nu f_{5/2})^{-1}_{5/2}$ nucleon configuration. The $17/2^-$ and $21/2^-$ states are related by a similar excitation of the $f_{5/2}$ neutron, now with the $(\pi h_{9/2})^6$ configuration coupling to 8^+ instead of 0^+.

4.2.1 Negative parity configurations

The excited states in the negative parity branch must be due to the pure $(\pi h_{9/2})^6 \otimes (\nu p_{1/2})^{-1}$ configuration or, to retain negative parity, the excitation of either a proton into the $f_{7/2}$ shell or moving the neutron hole from the $p_{1/2}$ shell to the $f_{5/2}$ orbital making an $f_{5/2}$ hole. Above the $21/2^-$ state there exist three $25/2^-$ states at 3138, 3282 and 3347 keV, the predominant configurations of which are suggested to be $(\pi h_{9/2})^6 \otimes (\nu p_{1/2})^{-1}$, $(\pi h_{9/2})^5 \otimes (\pi f_{7/2}) \otimes (\nu p_{1/2})^{-1}$ and $(\pi h_{9/2})^6 \otimes (\nu f_{5/2})^{-1}$ respectively. Here assignments have been based purely on agreement between experimental and predicted energies. The predictions place these states at 3007, 3259 and 3426 keV with RMS deviation of 112 keV from experimental values. The worst agreement ($\Delta E = 131$ keV) comes from the seniority four, $(\pi h_{9/2})^6 \otimes (\nu p_{1/2})^{-1}$, despite being at maximal coupling. This result is consistent with the closed shell ^{214}Ra case where the assigned pure $(\pi h_{9/2})^6_{12}$ configuration has a deviation of ΔE = 176 keV with the analogous 12^+ state. In ^{213}Ra, however, the prediction underestimates the energy of the $25/2^-$ state, while in ^{214}Ra the prediction over estimates the 12^+ state energy. This discrepancy is likely due to additional effects of configuration mixing in ^{213}Ra due to the additional $p_{1/2}$ valence neutron.

The $27/2^-$ and $29/2^-$ states, both attributed to the $(\pi h_{9/2})^5 \otimes (\pi f_{7/2}) \otimes (\nu p_{1/2})^{-1}$

[1]The core configuration will be mixed by pairing correlations to include components like $(\pi h_{9/2})^4 \otimes (\nu f_{7/2})^2 \otimes (\nu p_{1/2})^{-1}$

configuration have a RMS deviation of 54 keV, a twofold improvement over their $25/2^-$ counterparts . At this spin the $(\pi h_{9/2})^6 \otimes (\nu p_{1/2})^{-1}$ configuration ceases to contribute and, to get to higher spin, it is necessary to excite a proton into the $f_{7/2}$ shell thus reducing the effects of configuration mixing on these states.

4.2.2 Positive parity configurations

Excited states in the positive parity branch of the level scheme correspond to the excitation of a proton into the $i_{13/2}$ orbital giving the following configurations; $(\pi h_{9/2})^5 \otimes (\pi i_{13/2}) \otimes (\nu p_{1/2})^{-1}$ and $(\pi h_{9/2})^5 \otimes (\pi i_{13/2}) \otimes (\nu f_{5/2})^{-1}$. Discussion of the $23/2^+$ and $33/2^+$ isomeric states is left for the following sections.

The configurations of the $25/2^+$ and $27/2^+$ states are best matched energetically by the additional excitation of a $f_{5/2}$ neutron into the $p_{1/2}$ neutron hole thus creating an $f_{5/2}$ neutron hole. The spin and parity of these two states are therefore due to the re-coupling of the five $h_{9/2}$ protons as the both $i_{13/2}$ and $f_{5/2}$ will generally contribute their maximum available angular momentum. The best energetic agreement for the $25/2^+$ is given by the $(\pi h_{9/2})^5 \otimes (\pi i_{13/2}) \otimes (\nu f_{5/2})^{-1}$ configuration ($\Delta E = 41$ keV), however, the $27/2^+$ is closely matched by both possible positive parity configurations with a deviation of 123 keV for the same $f_{5/2}$ excitation and 211 keV for the $(\pi h_{9/2})^5 \otimes (\pi i_{13/2}) \otimes (\nu p_{1/2})^{-1}$ configuration. The possibility of configuration mixing at the $27/2^+$ state therefore gives rise to the lower experimentally observed energy of this excited state.

This configuration mixing at the $27/2^+$ state makes the cascade through positive parity states from the $33/2^+$ to the $23/2^+$ somewhat analogous to the cascade from the $17/2^-$ state to the ground state, although with greater level density as it is effectively an odd-odd (-odd) configuration. To clarify, the $23/2^+$ isomer can be treated as the ground state of this cascade as four of the valence $h_{9/2}$ protons couple to zero to give the minimum possible spin. The $25/2^+$ state is then produced in the excitation of the $f_{5/2}$ neutron not unlike the $5/2^-$ state above the ground state or, the $21/2^-$ state above the $17/2^-$ state. Above the $25/2^+$ state the remaining states (with the exception of the heavily mixed $27/2^+$ state) are produced by coupling the proton configuration with a $p_{1/2}$ neutron like the $9/2^-$, $13/2^-$ and $17/2^-$ states.

The $33/2^+$, as shown in Figure 4.1, can be produced through two different configurations. The $(\pi h_{9/2})^5 \otimes (\pi i_{13/2}) \otimes (\nu p_{1/2})^{-1}$ configuration places this state at 4379 keV while the $(\pi h_{9/2})^5 \otimes (\pi i_{13/2}) \otimes (\nu f_{5/2})^{-1}$ configuration places it at 4482 keV. The similarity in excitation energy of these two configurations means there is a significant level of configuration mixing and is thus responsible for the lower experimentally observed excitation energy.

4.2.3 The $23/2^+$ isomer

The 24.6(5) ns, $23/2^+$ isomer at 2609 keV is the lowest positive-parity state. It corresponds to the excitation of a proton into the $i_{13/2}$ orbital and has closest energetic agreement ($\Delta E = 119$ keV) with the $(\pi h_{9/2})^5 \otimes (\pi i_{13/2}) \otimes (\nu p_{1/2})^{-1}$ configuration. Such an assignment bears a close resemblance to the 11^- isomer in ^{214}Ra and is due to the same $i_{13/2}$ excitation with the coupling of the additional $p_{1/2}$ neutron hole. The lifetime of this state is in part due to it decaying via a low energy, E1 transition. The Weisskopf rate for such a transition corresponds to a lifetime of $\tau = 8$ fs which is six orders of magnitude lower than the measured lifetime of the 322 keV γ-ray this gives a transition strength of $2.9(6)\times10^{-7}$ W.u. For E1 transitions a hindrance factor of 3×10^6 is not without precedence in the trans-lead region [Gip75, Stu92, Mar12]. E1 transitions are absolutely forbidden in this valence space because the possible parity changing transitions correspond to $i_{13/2} \rightarrow h_{9/2}$ and $i_{13/2} \rightarrow f_{7/2}$, both of which require angular momentum changes of 2 and 3 $\hbar$, respectively.

4.2.4 The $33/2^+$ isomer

The high-spin 53.6(16) ns isomer decays via the emission of three transitions; a 41 keV M1, 606 keV M2 and 169 keV E2. The relative branching ratios are, however, heavily skewed towards the 41 keV transition which takes 84% of the intensity, and consequently the lifetime of the $33/2^+$ isomer is primarily due to this decay channel. M1 transitions within the same configuration ($(\pi h_{9/2})^5 \otimes (\pi i_{13/2}) \otimes (\nu p_{1/2})^{-1}$) are in general forbidden partially justifying the lifetime observed for the state. The overall hindrance of this state is also in part due to the *mid-shell cancellations* phenomenon where the E2 decay rate of a state is hindered when an orbital is half-filled. The excitation of the $h_{9/2}$ proton into the $i_{13/2}$ shell causes the occupancy of the $h_{9/2}$ shell to be 5 (half of its total, 2J + 1 = 10, capacity) thus giving rise to this effect.

Transition strengths for E2 transitions in neighbouring ^{214}Ra agree within order of magnitude with the measured transition strength of 50×10^{-3} for the 169 keV E2 (see Figure 3.4). There are, unfortunately no M2 analogues in ^{214}Ra to compare with the transition strength of the 606 keV M2, regardless, M2 transitions are generally hindered explaining the 606 keV γ-ray's poor competition with the parallel 41 keV

transition.

This isomer has no direct ^{214}Ra analogue although, therefore its isomerism is not purely brought about through nuclear structure. The configuration mixing due to the $(\pi h_{9/2})^5 \otimes (\pi i_{13/2}) \otimes (\nu p_{1/2})^{-1}$ and $(\pi h_{9/2})^5 \otimes (\pi i_{13/2}) \otimes (\nu f_{5/2})^{-1}$ reduces the excited state energy to the point where it can only decay via low energy transitions which will typically exhibit a longer lifetime.

4.3 Comparisons to similar nuclei

This section will investigate the structure of ^{213}Ra with reference to nuclei with similar nucleon configurations. The discussion will be primarily with reference to the closed neutron core ^{214}Ra but similar comparisons will be extended to the equivalent ^{212,211}Rn and ^{210,209}Po. These nuclei are equivalent in the sense that they both have even proton number and are the analogous N = 126 / N = 125 pairs, similar to ^{214,213}Ra. Discussions of level density and agreement with theoretical calculations will be limited to states in the following spin range: 8^+ / $(17/2^-)$ to 17^- / $(35/2^+)$ for the even (odd) nuclides.

Semi-empirical shell model calculations work best for nuclei with only a few particles outside the lead core. Consequently, the agreement between theory and experiment out of all the nuclei mentioned above is expected to be lowest for ^{213}Ra as it has the most valence nucleons. This is best shown through a comparison to ^{214}Ra. Figure 4.2 shows the relevant measured and theoretically predicted level schemes for ^{213}Ra and ^{214}Ra. Unsurprisingly ^{214}Ra shows better agreement, for states between the 17^- / $(35/2^+)$ and the 8^+/ $(17/2^-)$ isomers, with a RMS deviation of 123 keV (vs 139 keV for ^{213}Ra). It would be instructive to extend this type of analysis to the other N = 126 / (N = 125) isotopes in the future, when the present work is published.

The level density of ^{213}Ra is greater than ^{214}Ra beneath the $35/2^+$ state; this is due to the additional coupling of the $p_{1/2}$ and $f_{7/2}$ giving rise to a greater number of possible excited states. The most similar level density and structure is found in ^{211}Rn where the level scheme splits into a positive and negative parity branch before uniting again at a positive parity isomer. The level density in ^{211}Rn is comparable to ^{213}Ra, which is to be expected, as at low and intermediate spin the two

additional protons in Radium will typically be coupled to zero. Were this comparison taken to higher spin it would be expected that this increased level density in ^{213}Ra would persist to higher spin than in ^{211}Rn.

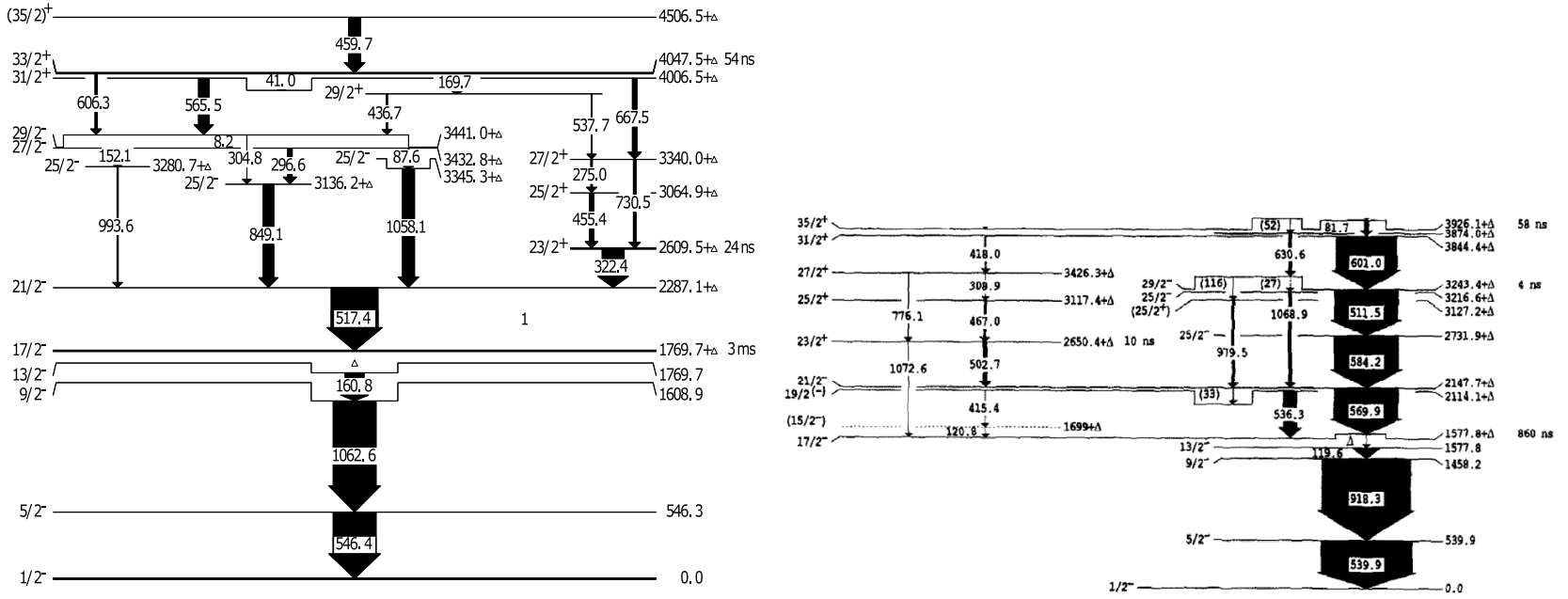

Figure 4.3: Level schemes for ^{213}Ra and ^{211}Rn. [Dav93]

The number of isomers present in the analogous spin range ($1/2^-$ to $35/2^+$) appears to decrease with the addition of more valence protons. Isomers in the trans-lead region are typically associated with low seniority states where component nucleons align to produce maximal coupling. The addition of two nucleons will increase the seniority and will thus lead to fewer isomeric states. This is a visible trend across the six selected nuclei where sub 8^+ / $(17/2^-)$ isomers are common each case. Figure 4.3 shows a definitive trend in the excited state energy for the same spin and parity states as more $h_{9/2}$ protons are added, corresponding to an increase in the effects of configuration mixing. In each case the $5/2^-$ state is produced in the same $p_{1/2} \rightarrow f_{5/2}$ excitation. The trend of increased isomer lifetime with increasing proton number again comes from the mid-shell cancellation effect.

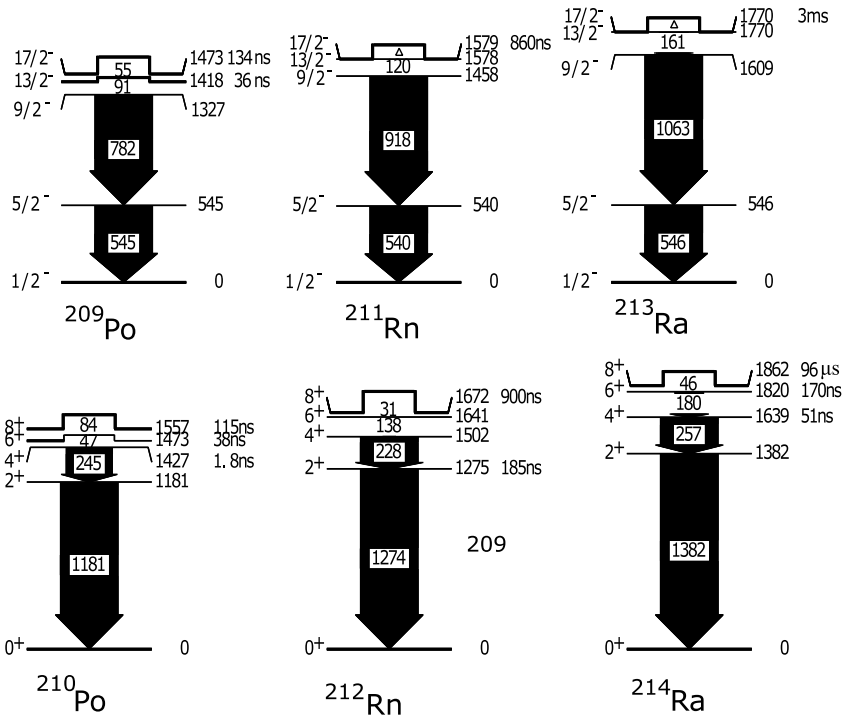

Figure 4.4: Partial level schemes for the relevant N = 125/N = 126 even-odd nuclei in the trans-lead region. The $5/2^-$ state in each case corresponds to the same $p_{1/2} \rightarrow f_{5/2}$ excitation.

Conclusions and future outlook

Using time-correlated γ-ray spectroscopy, detailed structural features of the level scheme of the nucleus ^{213}Ra have been revealed. Knowledge of ^{213}Ra has been extended up to 4.5 MeV and $J = 35/2\hbar$, including the identification of two new isomers. Using the γ-γ-ΔT method the lifetime of these states were measured at 24.6(5) ns for the $23/2^+$ isomer and 53.9(16) ns for the $33/2^+$ isomer. This work found no evidence of any higher-lying long-lived isomeric states.

Comparisons of theoretical predictions with neighbouring nuclei show that the agreement of semi-empirical shell model calculations and experiment degrades with the addition of valence nucleons, however, the calculations remain sufficiently accurate to build up an understanding of the nuclear structure and propose the dominant configurations. Furthermore, the systematic investigation of radium isotopes and N = 125, 126 neighbours has given insight into the evolving structures of these nuclei.

There is still much to learn about ^{213}Ra and indeed many nuclei in the trans-lead region. Future high spin studies of ^{213}Ra may observe the higher-lying isomers typical of nuclei in this region, however, such endeavours would require more than a three day experiment to gather the required statistics to successfully observe states above the $35/2^+$ state.

In summary, the present study of ^{213}Ra has probed the viability of the semi-empirical shell model moving further away from the ^{208}Pb core; this type of analysis should be extended to more neutron deficient nuclei where, so far, fission competition has limited the spectroscopic information available.

Bibliography

[Aud03] Audi, G., Wapstra, A., and Thibault, C. The ame2003 atomic mass evaluation: (ii). tables, graphs and references. *Nuclear Physics A*, 729(1):337 – 676, 2003. The 2003 {NUBASE} and Atomic Mass Evaluations.

[Bas07] Basunia, M. Nuclear data sheets for a = 213. *Nuclear Data Sheets*, 108(3):633 – 680, 2007.

[BEA67] BEARDEN, J.A. X-ray wavelengths. *Rev. Mod. Phys.*, 39:78–124, 1967.

[Blo71] Blomqvist, J., et al. Evidence for high-spin core-excited states in ^{210}po. *Physica Scripta*, 3(1):9, 1971.

[Byr86] Byrne, A.P. *The Nuclear Structure of High Spin States in ^{211,212,213}Fr.* Ph.D. thesis, Canberra, Australia, 1986.

[Dav93] Davidson, P., et al. Spectroscopy of ^{211}rn approaching the valence limit. *Nuclear Physics A*, 560(3):822 – 844, 1993.

[Fur87] Furley, D.J. *The Greek Cosmologists vol 1: The Formation of the Atomic Theory and its Earliest Critics.* Cambridge University Press, Cambridge, 1987.

[Gip75] Gippner, P., et al. A j-forbidden isomeric transition in ^{204}at. *Nuclear Physics A*, 237(1):142 – 148, 1975.

[Gre96] Greiner, W. and Maruhn, J. *Nuclear Models.* Springer-Verlag, New York, USA, 1996.

[Hax49] Haxel, O., Jensen, J.H.D., and Suess, H.E. On the "magic numbers" in nuclear structure. *Phys. Rev.*, 75:1766–1766, 1949.

[He04] Heberger, F., et al. Decay properties of isomeric states in radium isotopes close to n = 126. *The European Physical Journal A - Hadrons and Nuclei*, 22(2):253–260, 2004.

[Kib08] Kibdi, T., et al. Evaluation of theoretical conversion coefficients using bricc. *Nuclear Instruments and Methods in Physics Research Section A: Accelerators, Spectrometers, Detectors and Associated Equipment*, 589(2):202 – 229, 2008.

[Kra87] Krane, K.S. *Introductory Nuclear Physics*. John Wiley & Sons, Hoboken, New Jersey, USA, 1987.

[Lan95] Lane, G. *Coexistence and Structure of Deformed Shapes Near the Z=82 Closed Shell*. Ph.D. thesis, Australian National University, Canberra, Australia, 1995.

[Law80] Lawson, D. *Theory of the nuclear shell model*. Oxford University Press, New York, United States, 1980.

[Mar06] Martin, B. *Nuclear and Particle Physics*. John Wiley & Sons, Hoboken, New Jersey, USA, 2006.

[Mar12] Margerin, V. *Time Correlated Gamma-ray Spectroscopy and High-Spin Structure of the Odd-Odd Nucleus* ^{210}*Fr*. Master's thesis, Australian National University, Canberra, Australia, 2012.

[May49] Mayer, M.G. On closed shells in nuclei. ii. *Phys. Rev.*, 75:1969–1970, 1949.

[May50a] Mayer, M.G. Nuclear configurations in the spin-orbit coupling model. i. empirical evidence. *Phys. Rev.*, 78:16–21, 1950.

[May50b] Mayer, M.G. Nuclear configurations in the spin-orbit coupling model. ii. theoretical considerations. *Phys. Rev.*, 78:22–23, 1950.

[Mor76] Morinaga, H. and Yamazaki, T. *In-beam gamma-ray spectroscopy*. Elsevier North-Holland, Inc., New York, 1976.

[Ney94] Neyens, G., et al. "spin-lattice relaxation of ra in tl and g factor of the ^{213}Ra^{m}, τ=2.1 ms isomer". *Phys. Rev. C*, 49:645–649, 1994.

[Pol00] Poletti, A., et al. Core-excitations in ^{209}po. *Nuclear Physics A*, 665(34):318 – 331, 2000.

[Pol05] Poletti, A., et al. High spin states in ^{210}rn approaching the region of

3-particlehole neutron excitations. *Nuclear Physics A*, 756(12):83 – 117, 2005.

[Rad95] Radford, D. ESCL8R and LEVIT8R: Software for interactive graphical analysis of HPGe coincidence data sets. *Nucl. Instruments Methods Phys. Res. Sect. A Accel. Spectrometers, Detect. Assoc. Equip.*, 361(1-2):297–305, 1995.

[Rai76] Raich, D., et al. Gamma and alpha decay from the 2.1-msec isomer ^{213m}ra. *Zeitschrift fr Physik A Atoms and Nuclei*, 279(3):301–311, 1976.

[Ras76] Rasmussen, J., et al. Alpha decay theoretical calculations for 125-neutron nuclei. *Zeitschrift fr Physik A Atoms and Nuclei*, 279(3):313–317, 1976.

[RB07] R. Bengtsson, P.M. Nuclear physics: A non-disappearing magic trick. *Nature*, 449:411,413, 2007.

[Rie05] Rietz, R. *Effective Charges Near ^{56}Ni and Production of Anti-Nuclei Studied with Heavy-Ion Reactions*. Ph.D. thesis, Department of Physics, Lund University, Lund, Sweden, 2005.

[Ste80] Steffen, R. and K., A. Angular distribution and correlation of gamma rays, 1980.

[Stu92] Stuchbery, A., et al. Spectroscopy and shell model interpretation of high-spin states in the n = 126 nucleus ^{214}ra. *Nuclear Physics A*, 548(1):159 – 188, 1992.

[Stu03] Stuchbery, A.E. γ-ray angular distributions and correlations after projectile-fragmentation reactions. *Nuclear Physics A*, 723(1):69–92, 2003.

[Stu15] Stuchbery, A.E. *Unpublished Computer Code*. 2015.

[Tha66] Thackray, A.W. The origin of dalton's chemical atomic theory: Daltonian doubts resolved. *Isis*, 57(1):pp. 35–55, 1966.

[Tho04] Thomson, J.J. On the structure of the atom: an investigation of the stability and periods of oscillation of a number of corpuscles arranged at equal intervals around the circumference of a circle; with application

of the results to the theory of atomic structure. *Philosophical Magazine Series 6*, 7(39):237–265, 1904.

[Woo54] Woods, R.D. and Saxon, D.S. Diffuse surface optical model for nucleon-nuclei scattering. *Phys. Rev.*, 95:577–578, 1954.